UNIVERSITATEA "BABEȘ-BOLYAI", CLUJ-NAPOCA
FACULTATEA DE FIZICĂ
SPECIALIZAREA FIZICĂ COMPUTAŢIONALĂ

LUCRARE DE DISERTAŢIE

Coordonatori științifici
Lect. Dr. Zsolt Lázár
Ph.D. Franco Julio Mangiarotti

Absolvent
Gyopár Elekes

2020

Babeș-Bolyai University, Cluj-Napoca
Faculty of Physics
Specialization Computational Physics

MASTER THESIS

Stress Analysis of High Field Nb_3Sn Accelerator Magnets During Thermal Transients

Scientific advisors
Lect. Dr. Zsolt Lázár
Ph.D. Franco Julio Mangiarotti

Student
Gyopár Elekes

2020

Acknowledgements

Firstly, I would like to thank the opportunity to the CERN Technical Student Programme, which made possible to spend a very instructive and unforgettable period at CERN. During the time spent there, as a part of the HL-LHC project, I participated at the short model testing of the new Nb_3Sn focusing magnets.

I would like to express my gratitude to my supervisor, Ph.D. Franco Julio Mangiarotti, for his expertise, help and guidance during my internship at CERN and his support in completing my thesis.

I would like to thank Márta Bajkó, section leader of TE-MSC-TF, for inspiring my interest in superconducting accelerator magnets and her enthusiastic explanations to my questions.

I would like to extend my thank to the staff of SM18 (Magnet Test Facility) who were always opened to my enquiry and explained, with their professionalism, how the magnet testing is done inside CERN and how the instruments are working.

My internship at CERN was a life experience and I would like to thank everyone who helped to realize it and supported me in completing my dissertation.

Abstract

This thesis contains the study and results from my practical stage spent at the *European Organization for Nuclear Research* (CERN), where new technology Nb_3Sn superconducting magnets were tested for the Large Hadron Collider (LHC). The magnets, nicknamed MQXF, will be used for focusing the particle beams before and after the collision points.

Two short models (MQXFS4c and MQXFS6b) were tested in cryogenic conditions at SM18 (Magnet Test Facility) during my stay at CERN. The magnet testing has the main purpose to validate that they are working well according to the designed parameters. Among many other tests and measurements the stress inside the magnet is analysed. For magnets made with Nb_3Sn coils the level of stress is really important, because the superconducting coil can suffer irreversible degradation, if the stress reaches the critical values 150 - 200 MPa.

Stress analysis is already made on the magnets at fixed stages of magnet "lifetime" and fixed temperatures (e.g. coil assembling, after transportation, at low temperatures, during operations, after warm up). My task was to extend the stress analysis on the whole temperature range during thermal transients of magnet testing. This includes the cool-down of the magnets from room temperature to 1.9 K and the warming up back to room temperature. The cool-down process is crucial, because the components start to shrink by decreasing the temperature, which results in increased pressure inside the magnet and therefore on the coils.

The thesis discusses the stress evolution in function of time and temperature. The results of stress measurements are in good agreement with theoretical predictions, confirming that during thermal transients the coils of the magnets are not degraded.

Contents

Introduction

Curiosity is a main component of humankind. People were exploring their environment since the beginnings, creating instruments which ease their life, trying to understand how the world is working around them. Physics is a natural science, which has as main goal to understand and describe how the universe behaves. Physicists are studying the matter, its behaviour and its properties. During the centuries many sub-fields of Physics have appeared and along with the advances in theory, new technologies were also invented.

Particle Physics studies the smallest constituents of matter and radiation, including the fundamental interactions between them in order to explain their behaviour. The ancient Greeks already assumed that every matter is made of atoms, which means "indivisible". With the passage of time, scientist discovered that atoms are made of smaller particles: electrons, neutrons and protons. Nowadays we know that also neutrons and protons are formed by more elemental particles, like quarks. Modern particle physicists are focusing on the research of subatomic particles. The most current theory is the Standard Model, which explains the fundamental particles and fields, classifies the elementary particles. The theory describes the strong, weak and electromagnetic interactions. In order to prove the theory, scientists need experimental evidence, therefore experimental laboratories were created around the world. The main instruments to study the elementary particles are the particle accelerators. The field of Particle Physics is also called High Energy Physics.

CERN - European Organization for Nuclear Research - is well-known about the ongoing researches in the field of high-energy and particle physics. The acronym is originated from the French name - ***C**onseil **E**uropéen pour la **R**echerche **N**ucléaire*. CERN is one of the largest research facilities in the world, and the biggest in Europe, and it operates the largest and most powerful particle accelerator in the world. The organization was established in 1954, on the Franco-Swiss border, near Geneva, as an international collaboration, which today has 23 member states. The modern particle accelerators, like the Large Hadron Collider (LHC), enable scientists to study the fundamental laws of nature, however CERN is much more than a particle accelerator, a very large variety of experiments are taking place on site, while developing technologies enabling such complex machine building. Many scientists, engineers, physicists at CERN are dedicating their life to scientific researches and technology developments. Many fields have developments inside CERN and pushing the boundaries of technology, starting from electronics, sensors and robotics, through magnet technology, superconductivity and materials science until cryogenics, vacuum techniques or industrial controls and etc. These advancements contributes also to global improvements in medical technologies, aerospace applications, industry technologies, safety and more.

The LHC is a particle accelerator, which consists of accelerating structures and superconducting magnets; it has 27 km circumference and reaches 13 TeV energy at collision. Two particle beams are inside the accelerator, which travel close to the speed of light in opposite directions; the beams collide at the center of the four particle detectors - ATLAS, CMS, ALICE and LHCb. One of the main components of the particle accelerator are the magnets, which keep the accelerated particles on the right trajectory by strong dipolar magnetic fields. Quadrupoles and multi-polar magnets are used to correct the imperfections of the trajectory.

The next huge step in the life of LHC is the High-Luminosity Large Hadron Collider (HL-LHC) project. The luminosity is an indicator number, which is proportional to the number of collisions at given time in the accelerator. The purpose of this project is to increase the number of collisions inside the detectors in order to have more data about the less frequent, but most interesting events at particle collisions, like detecting Higgs-bosons. In the frame of the HL-LHC project, during the next years some main components of the accelerator will be replaced by new technology components with better performance, aiming to increase the luminosity by a factor of 10.

This thesis will focus on the new quadrupole magnets, which are responsible for focusing the beams before and after the experiments. By squeezing the particle beams, the cross-section decreases, resulting in higher density of particles and therefore an increment in the probability of collision at the intersecting points. The quadrupoles will be made with Nb_3Sn type superconducting coils, which have better performance than the $NbTi$ magnets used until now, Nb_3Sn coils will provide 11.4 T peak magnetic field with 150-mm-aperture (1). This new Nb_3Sn magnets have very delicate process of manufacturing. The superconducting Nb_3Sn material results from a chemical reaction at 600° C, while the operating temperature of the superconducting magnets in the LHC is 1.9 K, therefore the used materials have to resist a very big temperature range, without loosing their characteristics and performance. Because the Nb_3Sn is really brittle, the stress has also an impact on the properties and performance of the magnet. When the magnets are cooled down from room temperature to their operating temperature, the magnet shrinks and the stress increases on the magnets coils. If the superconducting coils reach a critical value of stress, they could suffer permanent degradation.

These new quadrupoles are nicknamed MQXF magnets. They are designed and constructed in an international collaboration with laboratories: Lawrence Berkeley National Laboratory (LBNL), Fermi National Accelerator Laboratory (FNAL), Brookhaven National Laboratory (BNL) from USA. The short models (MQXFS) for validating the magnet design were already fabricated and tested. This thesis will study the evolution of the stress values inside two short model magnets registered during the cool-down and warm-up processes (thermal transients). The measurements took place on site of CERN, at the Magnet Test Facility called SM18. The thesis accompanies the lifetime of a superconducting magnet, from the magnet design and technological part of manufacturing, through instrumental equipment of magnets for data acquisition until data processing and discussion of test result.

The structure of this work is the following:

1. High Energy Physics - contains a general presentation of the field of particle physics, also known as high energy physics. Describing the principles of an particle accelerator. Presentation of the main structure of the LHC with some details about the upcoming upgrades.

2. Aspects of superconducting magnet design - This chapter contours how complex process is to design, produce and validate superconducting magnets. Some related fields are briefly presented.

3. New technology: Nb_3Sn superconducting accelerator magnets - This chapter presents the description of the structure and parameters of the new quadrupole magnets. For the Nb_3Sn coils the stress has a main impact on the magnet's performance.

4. Magnet testing - Includes the main steps of magnet testing and the presentation of SM18 test facility, where both model magnets and series magnets are tested at cryogenic conditions. Description of the sensors for measuring strain and temperatures on the new Nb_3Sn quadrupole magnets will be given.

5. Study of strain and stress - for the Nb_3Sn magnets the stress has an major influence on the performance. This chapter includes the study of stress in case of the new quadrupoles. The main focus is on the evolution of the stress during the cool-down and warm-up processes, named thermal transients.

6. Magnet test analysis and discussion - This chapter contains the measurements and results obtained on two short model MQXFS4 and MQXFS6 magnets, and compared with the theoretical expectations and validating the test process, proving that the magnets does not degrade during tests. The discussion part presents the parameters which can influence the stress evolution inside the magnets during thermal transients.

Conclusions - includes the main results and ideas deducted from the measurements of short model magnets.

Chapter 1

High Energy Physics

Particle Physics, also known as High Energy Physics (HEP), studies the most elementary constituents of matter. Physicists try to understand the mechanism and interaction of these elementary particles and describe their behaviour by theories and models. Nowadays the Standard Model is at the basis of particle physics.

The Standard Model

This model was developed in the second half of the 20^{th} century and it explains successfully almost all physics experimental results. It confirms that the universe is built from a few basic fundamental particles, which are governed by fundamental forces. The model uses quantum field theory at its basis. The elementary particles can be classified into two basic types: fermions (they have half-integer spin, using Fermi-Dirac statistics) and bosons (integer spin, Bose-Einstein statistics). The table of the elementary particles can be seen on fig. 1.1.

The fermions can further grouped into quarks and leptons, each with 6 elementary particle from different generations. All the matter is built up from particles from the first generation (up and down quarks, electron and electrons neutrinos). The other generation particles are not stable, they decay to the more stable ones.

The fundamental forces are the gravitational, strong, weak and electromagnetic forces. Except the gravitational force, the Standard Model connects the forces with corresponding bosons: the gluon is the carrier of the strong force, the electromagnetic force is carried by the photon, while the weak force is related to the W and Z bosons.

The Standard Model has successfully predicted the interactions between quarks and leptons and other phenomenons. Physicists can prove, better understand and further explore the model using experiments.

European Organization for Nuclear Research

CERN is an international research institute based in Europe, also known as European Laboratory for Particle Physics, where a huge number of physics experiments take place. A large number of physicists, engineers and technicians from different countries around the world are studying the fundamental physics at CERN, focusing on the basic constituents of matter of the universe. CERN operates the largest particle accelerator in the world, the Large Hadron Collider (LHC). In the LHC protons and also heavier ions are accelerated almost to the speed of light and they circulate in two beams in opposite direction. These particle beams cross each other at the place of the 4 experiments, adding up their energy and recreating the conditions after the Big Bang. From particle collisions the subatomic particles

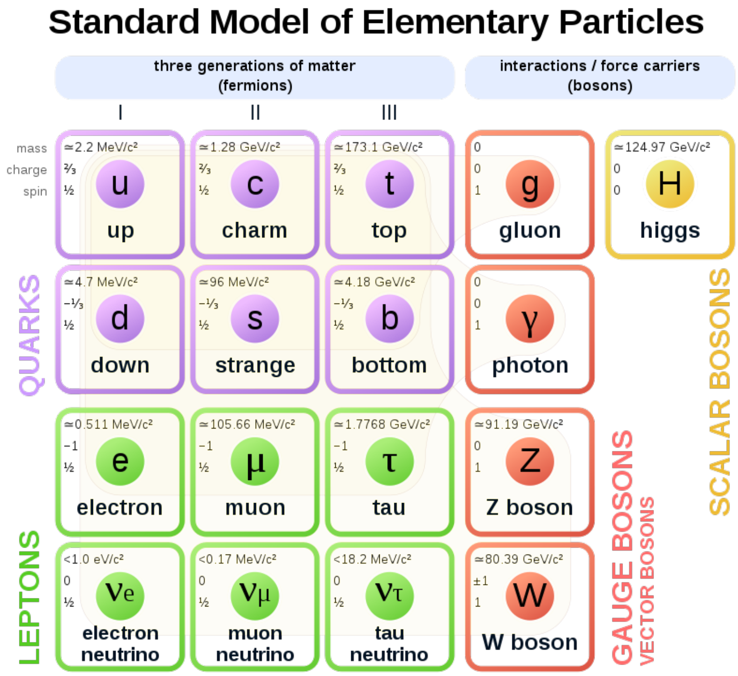

Figure 1.1: Elementary particles of the Standard Model (2)

can be detected and studied, this experiments contributes to prove and further develop the theoretical models.

1.1 Large Hadron Collider

The Large Hadron Collider (LHC) is the main instrument for Particle Physics and High Energy Physics research at CERN. The LHC is located on the border of Switzerland and France. The LHC is the largest particle accelerator with it's almost 27 km main ring, 100 metres underground and it is the coolest place in the Universe at its operating time, when the system is cooled down to 1.9 K. This low temperature is needed for the superconducting magnets, which are one of the main components of the LHC ring. The LHC accelerates particles up to 6.5 TeV and when the two particle beams with opposite direction collide, reach the 13 TeV center-of-mass energy at collision. More technical detail can be found in the design report (3). The LHC has 4 main experiments ATLAS, ALICE, CMS and LHCb, there are also three smaller ones called: LHCf, TOTEM and MoEDAL.

ATLAS - A Toroidal LHC ApparatuS
It is a general-purpose detector, which investigates wide range of physics. This detector is the largest one. The detector is made from six subsystems, designed to detect some of the tiniest particles. The opposite directed particle beams collide inside the detector; the resulting new particles will propagate in all directions. The system can record the trajectory, the momentum and the energy of the particles and make possible to identify them.

CMS - Compact Muon Solenoid
It is also a general purpose detector, just like the ATLAS, however uses different magnet-system design and technological solutions. It is designed to study any new physics phenomena, with several concentric layers of components, which help to analyse particles coming from any directions from the collision point. It can bend the trajectory of particle, identifying their tracks and measure their energy. As the name shows, the CMS can directly observe muons.

ALICE - A Large Ion Collider Experiment
This detector is a heavy-ion detector, which is designed for strongly interacting matter. It can study quark-gluon plasma, which is a state of matter thought to have formed just after the Big Bang. The ALICE collaboration is investigating why protons and neutrons have a mass 100 times larger than their building blocks, the quarks. They are trying to find out if the quarks inside can be freed or not.

LHCb - Large Hadron Collider beauty
The LHb detector makes possible to investigate the differences between matter and anti-matter. The members of the LHCb collaboration are studying the beauty quarks (b quark), which decay very quickly, therefore a very sophisticated series of sub-detectors were created for detecting these particles.

The TOTEM and LHCf uses the detectors on either side of CMS and ATLAS respectively, and they study the protons and heavy ions. The MoEDAL is searching for magnetic monopoles near to the LHCb experiment.

Structure of the LHC

The exact structure of LHC can be seen on fig. 1.2, it is not a perfect cycle: it has eight arcs, eight long straight sections and two transition regions (called "dispersion suppressors") on each end of the long straight sections. One long straight sections with two transition regions is called an "insertion" (4).

A sector is the part between two insertion points, the eight sectors of LHC are independent working units. The installation and hardware commissioning happens sector by sector. The dipole magnets are also connected electrically in series and in the same cryovolume inside a sector, so they are powered independently (4).

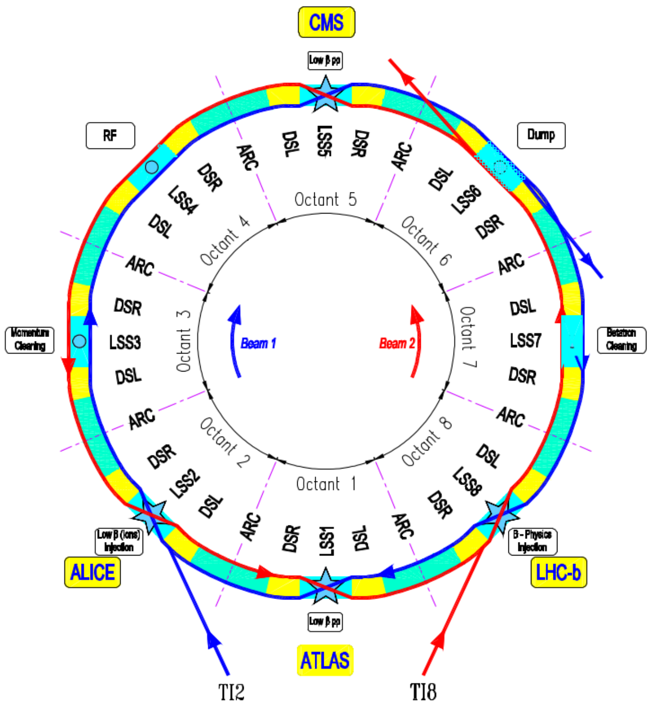

Figure 1.2: The structure and the main octants of the LHC (3). The arcs contain the bending dipole magnets, the long straight sections (LSS) have specific purposes and on each side (left, right) they have a transition region, called dispersion suppressors (DS).

An octant starts from the middle of an arc and ends in the middle of the following arc (4) and each long straight section inside an octant has different purpose:

- Point 1 - ATLAS experiment
- Point 2 - ALICE experiment and injection
- Point 3 - beam cleaning
- Point 4 - radio-frequency (RF) cavities - giving energy to particles
- Point 5 - CMS experiment
- Point 6 - dumping system - extraction of particle beam
- Point 7 - beam cleaning
- Point 8 - LHC-b experiment and injection

The main elements of the particle accelerator are (4):

- the **vacuum tube** - where the particles circulate, ensuring that the accelerated particles do not collide with gas molecules,
- the **electromagnets** - for guiding the particles through the vacuum tube, focusing the particle beams and correcting the trajectory,
- the **accelerating cavities** - to increase particles' energy to the collision energy and to keep it constant at that level.

Accelerating process at CERN

For accelerating particles radio-frequency (RF) cavities are used in the LHC. The acceleration of the particles is done in many stages made consecutively, which increase the energy of the particles gradually, each in a different machine. The energy reached after the accelerating steps can be found in table 1.1. In the LHC usually protons are accelerated, which are part of the hadron class in the Standard Model, but lead ions can also be accelerated.

Step	Accelerator	Energy	Velocity[%] of c	Radius[m]
1.	LINAC2	50 MeV	31.4	
2.	PS Booster (PSB)	1.4 GeV	91.6	4 x 25
3.	Proton Synchrotron (PS)	25 GeV	99.9 3	628
4.	Super Proton Synchrotron (SPS)	450 GeV	99.9998	6900
5.	LHC	7 TeV*	99.9999991	26 659

Table 1.1: Accelerating steps from ring to ring (4) for protons, *designed value (actual 6.5 TeV)

The journey of the protons begins from a bottle of H_2 gas, the molecules are pumped into the LINAC2 system and then the electrons are captured with an electric field in the injector section of the linear accelerator. The protons continue their path to a linear accelerator, where the particles are accelerated with electromagnetic fields. At the end of the linear acceleration the protons already have 50 MeV energy (6).

The next step is the PS Booster, which has 4 rings one above each other. Here the acceleration is done in pulses by radio-frequency cavities and the trajectory is kept circular by electromagnets. At the end of the acceleration in the PS Booster the protons already have 91.6 % of the speed of light, an energy of 1.4 GeV (6).

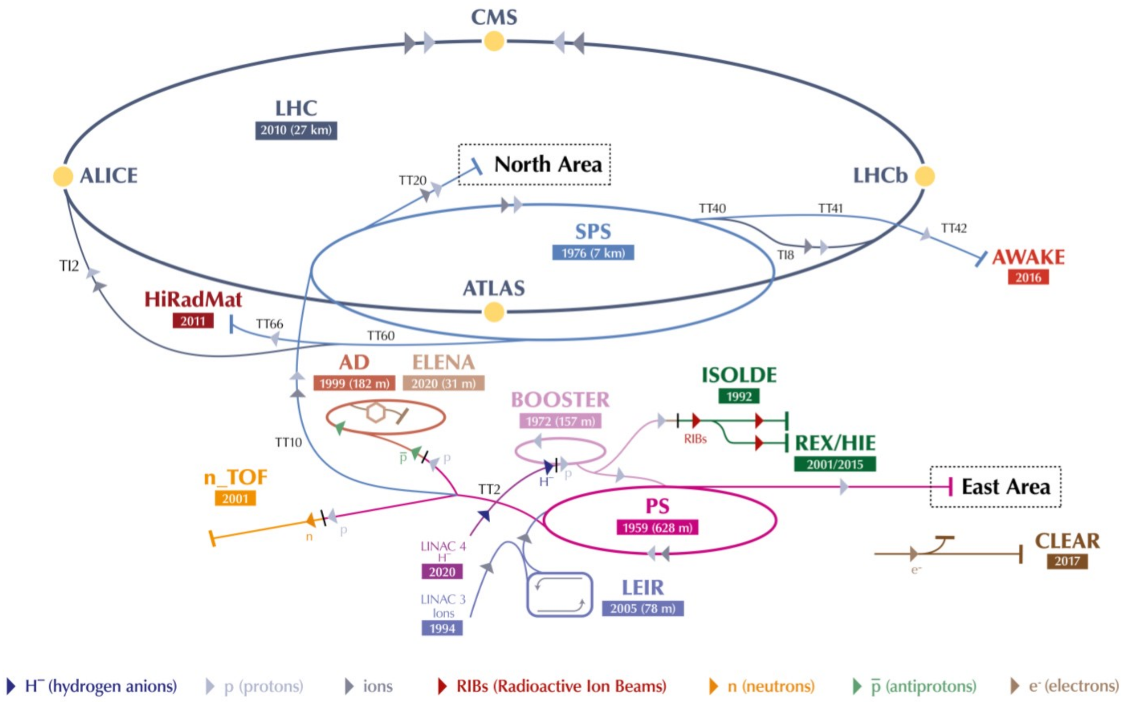

Figure 1.3: CERN Accelerating Complex (5)

From the Booster the protons go to the Proton Synchrotron (PS) for further acceleration. The particles reach 25 GeV energy here. In the PS alpha particles (helium nuclei), oxygen and sulphur nuclei, electrons, positrons and anti-protons can be also accelerated (6).

After the PS the protons are injected to the Super Proton Synchrotron (SPS) where the energy is increased up to 450 GeV. The SPS has 1317 conventional electromagnets on nearly 7 kilometres in circumference (6).

The last stage of the acceleration complex is in the LHC, where the protons reach 6.5 TeV energy per beam. At the time of the collisions the energy of the two beams adds up and it results in 13 TeV center-of-mass energy (6).

A number of $1.2 \cdot 10^{11}$ protons are injected to the accelerator per bunch and two opposite direction beams contains 2808 bunches each. They make over 11000 turns per second in the LHC tunnel and approximately make 1 billion collisions per second (3).

This accelerating chain can be also used for other experiments not located in the LHC. After some of the accelerating steps there is a possibility to redirect the particle beam to small specific experiments, which studies different things based on the already reached energy range. The arrangement of the accelerators and experiment are illustrated on fig. 1.3. For example, after PS the particles go to the Antiproton Decelerator (AD) or to Extra Low Energy Antiproton decelerator (ELENA).

Magnets in the LHC

The main characteristics of a circular accelerator are the **energy** and the **luminosity**. The most simplified equation for designing a circular particle accelerator is (7):

$$E = 0.3 \cdot B \cdot r, \tag{1.1}$$

where E is the energy, B is the magnetic field and r is the curvature of the trajectory of the particles. This equation shows that in order to reach higher energies we have two possibilities: we need to increase the magnetic field or we need to increase the bending radius of the particle's trajectory. In other words: the limit is the strength of the **dipole magnet** field which bends the particle beam, or the cost of the tunnel hosting the accelerator.

The **luminosity** is an indicator number for the accelerator's performance, it is proportional with the number of collisions per unit time. The peak luminosity is defined as (1):

$$L = \gamma \frac{n_b N^2 f_{ref}}{4\pi\beta^* \varepsilon_n} R \tag{1.2}$$

, where γ is the relativistic gamma factor; n_b is the number of bunches per beam colliding at the interaction points; N is the number of particles per bunch; f_{ref} is the revolution frequency; β^* is the beam beta function at the collision point; ε_n is the transverse normalized emittence; R is a luminosity geometrical reduction factor from the crossing angle (1).

Higher luminosity means a more powerful tool, producing more data for physicists. The luminosity depends on the beam intensity, geometry, the energy and length of the machine. Ultimately focusing the particle beams increases the luminosity. In the LHC **quadrupole magnets** are used for squeeze the beams. Although is not very intuitive from the formula, here the limit is the aperture of the magnets, which can be translated again to higher magnetic fields.

The use of conventional magnets is not feasible in the case of high energy particle accelerators. Superconducting magnets are used in order to reach high energies and luminosity. Superconductors have the advantage of minimal power consumption (for the cooling process), high current density and achieving high magnetic fields. We can reduce the bending radius by using superconducting dipoles, this decreases the size of the accelerator (cost). The luminosity can be increased using also superconducting quadrupoles, which can have larger apertures and can have proper gradient for focusing the particle beams.

In the LHC accelerator there are around 9600 magnets in total, with a large variety: dipoles, quadrupoles, sextupoles, octupoles, decapoles, corrector magnets etc. These magnets are responsible for the optimizations of the particle's trajectory. 1232 superconducting dipoles are placed in the tunnel for bending the particle beam, while the 392 quadrupoles are distributed along the ring to keep the beam focused (4). Further 32 large aperture quadrupoles are used for strongly focusing the beam before and after the interaction regions. More detail on the used magnet types in the accelerator can be found in (8).

The peak magnetic field of the currently used $NbTi$ dipole magnets in operation is 8.3 T, and the peak luminosity of the LHC is $1.2 \cdot 10^{34} cm^{-2} s^{-1}$ (1).

1.2 High Luminosity - LHC (HL-LHC)

One of the main parameters of a particle accelerator, as mentioned before, is the luminosity. The luminosity shows the number of collisions per second what can be produced in a detector per 1 cm^2. The ongoing developments at CERN in the frame of the HL-LHC project are focused on reaching higher luminosity, the goal is to increase the luminosity of the present LHC by a factor of 10. According to the HL-LHC upgrade many magnets, such as dipoles, quadrupoles and corrector-magnets will be replaced near the main experiments - ATLAS and CMS.

During the High Luminosity project more than 100 new magnets will be constructed of 11 different types. The cross-sections of these magnets can be seen on fig. 1.4. These magnets will be realized via 6 international collaborations (10). Some of the new magnets are in the R&D phase while other models have already been produced and tested in cryogenic conditions. The replacement of the magnets is estimated to be done 2025 - 2027.

The **Interaction Region (IR)** includes all the magnets before and after the detectors, including dipoles, quadrupoles and corrector-magnets. The IR - magnets have the purpose

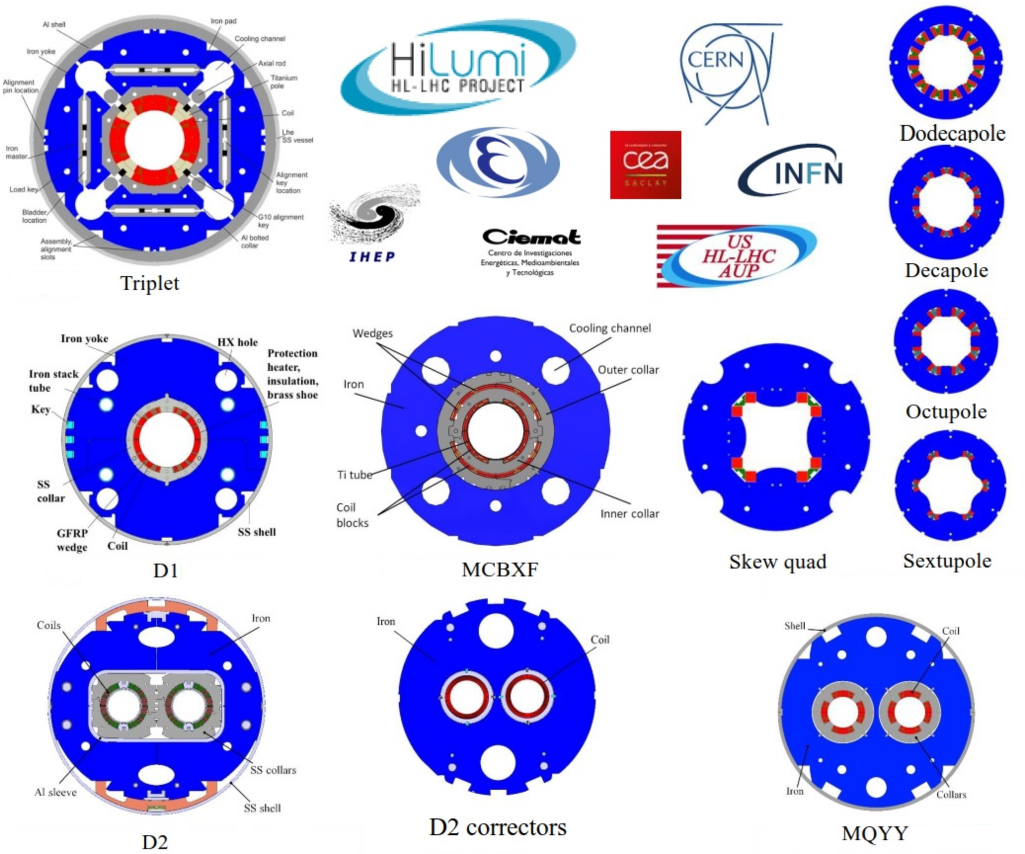

Figure 1.4: Cross-section of superconducting magnets with different types, which will be placed in the interaction region of the HL-LHC (9). The Triplet is the nickname of the focusing magnets in the interaction region, which will be made of Nb_3Sn.

to align and focus the particle beams properly before reaching the collision points at the center of detectors.

The focusing magnets used in the LHC currently are all made of $NbTi$. These focusing quadrupoles reach magnetic fields around 8-9 T (3) and have 70 mm aperture. During the upgrade of the LHC of the interaction zone these final focusing magnets will be replaced by Nb_3Sn magnets, the magnetic field created by these magnets can reach the 11.4 T (1) and they can provide proper magnetic field gradient 132.6 T/m (more information in section 3.2) for 150 mm aperture. MQXF magnets will be placed before and after the ATLAS and CMS detectors. These magnets are also called the inner triplet (Q1, Q2, Q3).

The purpose of the new triplet magnets is to increase the collision rate of the particles resulting in increased amount of data to analyze. The higher collision rate is achieved by:

- increasing the aperture of the quadrupoles in order to collect more particles after the collision points (having more particle further in the tunnel) and
- focusing the particle beam, which means that they reduce the diameter of the circulating particles so the density will increase. The higher the density of the particles inside the beam the higher the probability of collisions, means higher luminosity.

Chapter 2

Aspects of superconducting magnet design

For experiments in particle physics: high energy and complex systems are needed. Both for the accelerators and experiments a key component is the magnet system. For accelerators we need compact multi-polar magnets to reach high magnetic field, while for experiments very large dimensions are required to be able to observe the particles created after a collision. To create magnets with larger magnetic fields, superconductor materials are used. The core of a superconducting magnet is the coil, which is made from superconducting conductors. An electric current can flow through the superconductor wire with no dissipation. Superconductors have the advantages to create high magnetic fields and operate with high current densities. The superconducting magnets can be operated with minimal power consumption used only for the refrigeration power. Superconducting magnets are used not only in particle accelerators but also in spectrometers, in hospitals (MRI machines), fusion reactors and even for the railway systems (MAGLEV).

Designing and producing a superconducting magnet is real challenge and it is very complex process. Designers must take into account the magnet mechanics, electrodynamics, cryogenics and superconductor physics. There are theoretical and technological constraints as well. In this chapter I will highlight the most important aspects which need to be considered during a magnet design and construction.

2.1 Superconductivity

The discovery of superconductivity can be dated to 1911, when Heike Kammerlingh Onnes was studying the resistance of many materials at cryogenic temperatures, using liquid helium. In an experiment he observed that the resistance of the mercury at 4.2 K abruptly disappears. Later on superconductivity was observed also in other materials. In 1933 scientists discovered that also the magnetic fields are expelled in superconductors, this phenomenon is called the **Meissner-effect** or Meissner-Ochsenfeld effect.

The first theoretical model for superconductivity using classical physics could explain the Meissner effect. The **London equations** were based on Newton's second law applied for the superconducting electrons.

In the 1950s two further theory appeared for describing superconductivity: **Gingsburg-Landau theory** - a phenomenological theory, which combined second-order phase transition with a Schrödinger-like wave equation and **Bardeen-Cooper-Schrieffer (BCS) theory** - a complete microscopic theory, with the concept of Cooper pairs (electrons interacting through phonons), explaining the superconducting current as a superfluid of these Cooper-pairs .

Superconducting materials

Many of the chemical elements posses superconducting properties, but only a few of them are suitable to produce superconducting wires for practical purposes.

The operating conditions to keep the superconducting properties of a given material are the following:

- the critical temperature (T_c)
- the critical current density (j_c)
- the critical magnetic field (H_c)

These three parameters define the so called critical surface, below which the materials preserve the superconducting state.

The superconducting materials can be classified depending on their critical temperature in **LTS** - low temperature superconductors and **HTS** - high temperature superconductors. The limit between high and low temperature is around 120 K by convention. Nowadays LTS superconductors are widely used in large scale applications, but are many advancements for HTS materials too. For the future of the superconductor technology the HTS represents a new opportunity.

Another classification of superconducting materials is **Type-I** and **Type-II** superconductors, for both types, below a given H_c the magnetic field do not penetrate. In case of Type-I superconductors the superconductivity simply disappears when the applied magnetic field is to high ($> H_c$). While Type-II superconductors have two critical magnetic fields. After exceeding the H_{c1} the material still remains in superconducting phase, and magnetic flux vortices appear and penetrate the material. The density of such vortices becomes higher by increasing the magnetic field and when is exceeds the H_{c2}, the material loses the superconductivity phase.

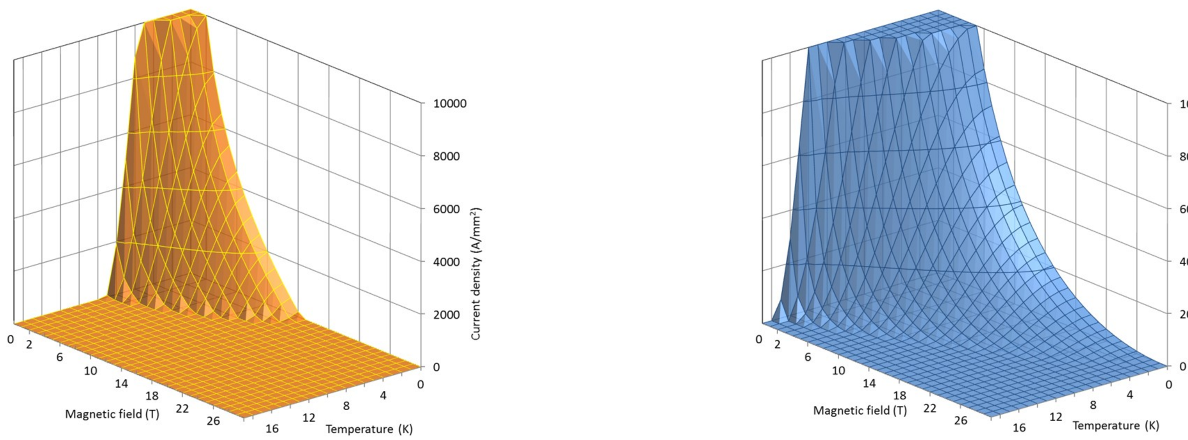

(a) $NbTi$
$T_c = 9.8$ K; $B_{c2} = 14.5$ T

(b) Nb_3Sn
$T_c = 18.05$ K; $B_{c2} = 28$ T

Figure 2.1: Critical surface of $NbTi$ and Nb_3Sn superconducting materials (11). The critical surface is defined by the three critical parameter: temperature (T_c), current density (j_c), and magnetic field (H_c).

The two most commonly used superconducting materials in practice are $NbTi$ and Nb_3Sn, both LTS and Type-II superconductors. The technology for producing $NbTi$ superconductor components is advanced at a mature stage. The Nb_3Sn has higher critical parameters, but it is a very brittle material. The fabrication process of such material is quite complex and delicate. The critical surface of these materials can be seen on fig. 2.1.

The fabrication process from the superconducting material to a final electromagnet is long and needs to be designed properly. The magnet design starts with defining the appropriate material with the required properties. With that material the first step is to make strands, wires and then cable. From the superconducting cables coils can be wounded. The coils are kept together with the help of the "collars", while the magnetic field lines are guided inside the surrounding iron yoke. The while assembly is encapsulated into a stainless steel cylinder, that becomes the Helium container of the magnet. The simplified steps of magnet fabrication is shown on fig. 2.2.

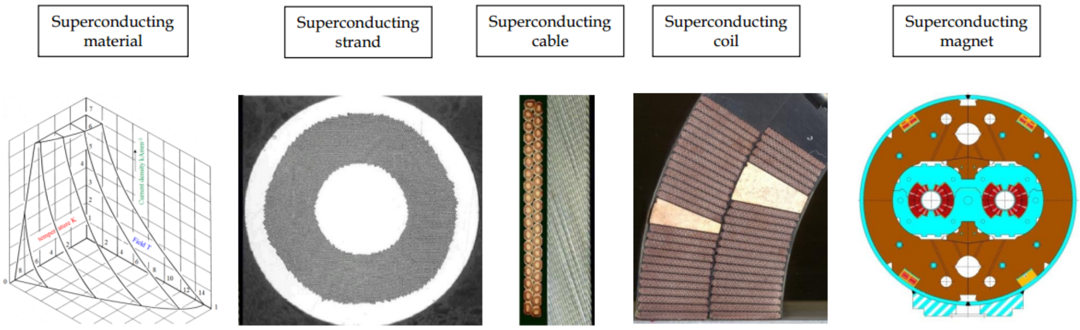

Figure 2.2: The simplified steps of superconducting magnet fabrication (11).

2.2 Superconducting strands and cables

Superconducting cables are not made from pure superconducting material, the superconductors are combined with conventional conductors. Firstly the material is produced in small filaments and surrounded by a stabilizer (e.g. Cu) to form a multi-filament wire or strand (see fig. 2.3a). The typical diameter of a strand is 0.5-1 mm. The ratio of superconducting material and copper in a wire is around 0.25-0.3 (11). The use of a stabilizer is necessary to cope with undesired transiting of the superconductors to normal stage.

The next step is to use multiple wires in order to form multi-strand cables. Most of the superconducting coils for High Energy Physics applications are made from **Rutherford cables** (see fig. 2.3b), which are designed in order to increase the performance.

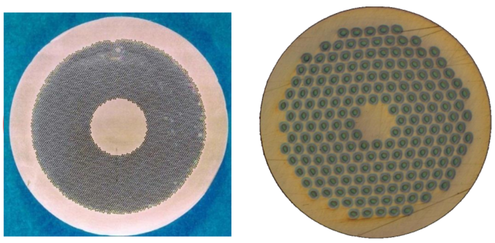

(a) $NbTi$ (left) and Nb_3Sn (right) wires

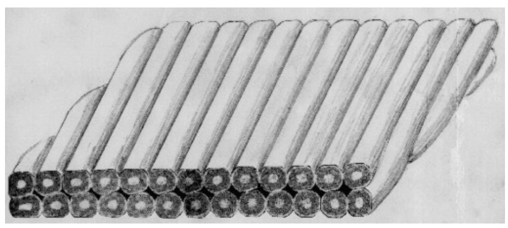

(b) Rutherford cable

Figure 2.3: Strands and cables used for superconducting magnets (11).

2.3 Magnetic design

In particle accelerators two main types of superconducting magnets are used dipoles and quadrupoles. The shape of the created magnetic field can influence the motion of a charged particle in different ways. The dipoles have the purpose of bending the particle beam trajectory and are directly correlated with the energy of the accelerator - a particle with higher energy needs a larger magnetic field to keep it on the same orbit. The quadrupoles are focusing the particle beam, both to keep the beam confined inside the accelerator and to increase the luminosity of the accelerator (number of collisions).

The dipole consists in two magnetic poles, which are wounded from superconductor cables according to figure 2.5a. The field lines create a homogeneous vertical field, which steers the particles on a horizontal circular orbit according to the Lorentz-force applied on the moving charged particle.

The quadruples have four magnetic poles, the field lines can be seen of fig. 2.5b. The created field in the center equals to zero, therefore the particles are repelled by the gradient lines to the center. The quadrupole has the effect to focus the particle beam in one direction (e.g. horizontal), but de-focus it in the other direction (e.g. vertical). In order to get the net focusing in both directions, the quadrupoles need to bee placed one after the other with alternating polarities.

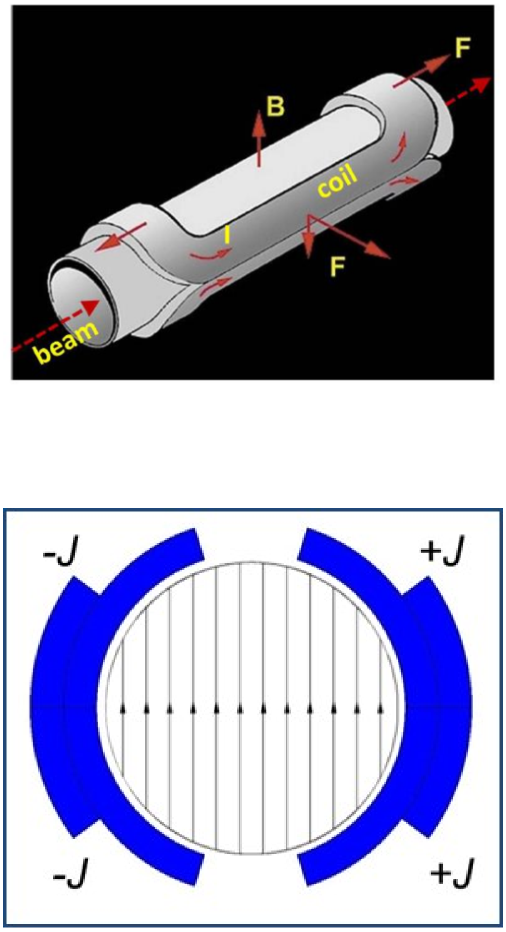

(a) Dipole

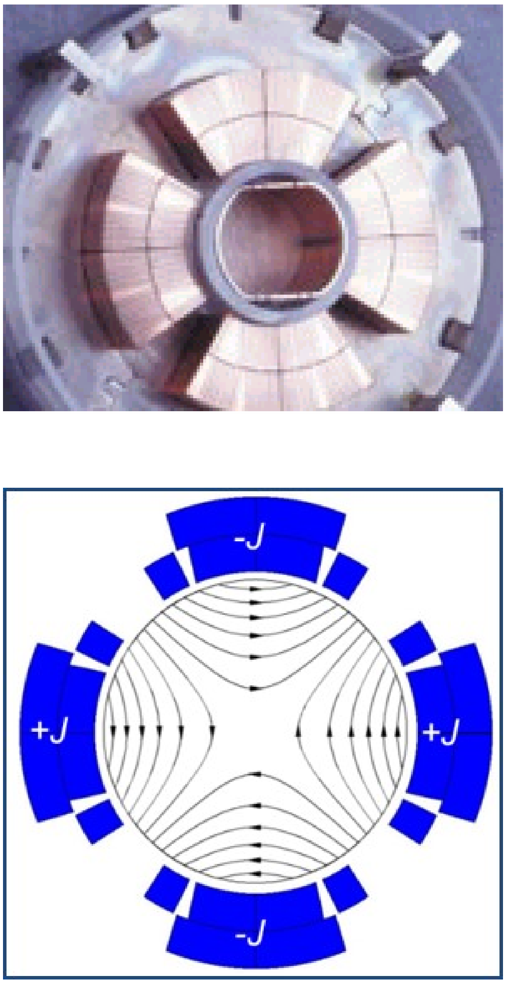

(b) Quadrupole

Figure 2.5: Magnetic field created by dipole and quadrupole magnets (11)
Dipoles are bending the particle trajectory, quadrupoles are for focusing the particle beam.

2.4 Mechanical design

On a particle in electromagnetic field the **Lorentz-force** [N] is applied:

$$\vec{F}_L = q(\vec{E} + \vec{v} \times \vec{B}) \quad (2.1)$$

, q - electric charge of the particle, E - electric field, v - velocity, B - magnetic field.

Similarly, a conductor element is subjected to a force density $[N/m^3]$

$$\vec{f}_L = \vec{J} \times \vec{B}$$

, J is the current density$[A/mm^2]$

The electromagnetic forces in a dipole or quadrupole magnets are pushing the coils toward the mid plane in vertical direction and outwards in the horizontal direction. At the end of the coils the forces pull the coils longitudinally. The stress resulting from the electromagnetic force can damage the magnets. For Nb_3Sn coils the conductor can suffer degradation at 150-200 MPa.

These large forces are taken by the magnet's support structure. This structure also has the role to provide a required pre-stress to the coil, to reduce conductor motion and to retain the liquid Helium (LHe). The elements of the support structure are indicated on figure 2.6:

- collar - stainless-steel or aluminium lamination clamping the coils. They provide coil pre-stressing, rigid support against the electromagnetic forces and precise cavity.
- iron yoke - contains and enhances the magnetic field, also contributes to the rigidity and limits radial displacement.
- shell - is the most outer part of the magnet, containing the cold mass and it is the main body of the LHe container. The shell can be composed by two half shells of stainless steel welded around the yoke, which gives rigidity and pre-compression.

During cool-down the components shrink differently according to their thermal contraction coefficients and cause significant variations of coil stress. The differential-thermal contractions are such that, if not properly considered by the magnet designers, once in operational conditions the magnets are exposed to be deformed and ultimately destroyed with the appearing Lorentz forces.

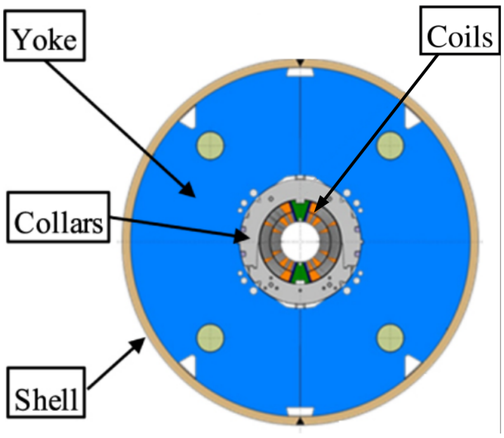

Figure 2.6: Cross-section of the Nb_3Sn 11T dipole magnet (12). The mechanical structure has the purpose to restrain the Lorentz forces, which tend to repel the coils.

2.5 Magnet quenching

When a small part of the superconducting material enters the normal resistive state, it is called quench. A quench is caused by exceeding the critical value of at least one of the parameters T_c, j_c, B_c. The origin of the quench can be:

- mechanical: frictional motion, epoxy cracking
- electromagnetic event: flux-jump, AC losses
- thermal: degraded cooling
- nuclear events: particle showers

A quench results in a rise in temperature due to Joule heating caused by the large amount of current flowing in the resistive part (copper) of the cables. When the magnet quenches at a spot, the heat is propagating from the starting point and causes a chain reaction. If left unattended, the superconducting coil can melt and permanently damaged after a quench, therefore quench protection systems were developed in order to save the coils.

The amount of energy stored in the magnet is $W = \frac{LI^2}{2}$, where L is the inductance of the magnet and I is the current flowing through. The stored energy of a superconductor magnet can reach millions of joules. In the case of quench the powering of magnet should be interrupted immediately (< 1 s) and the stored energy in the magnet should be extracted or dissipated in a volume of the magnet. The methods for quench protection are the use of external dump resistor, placing quench heaters on the coils or the most recent developed CLIQ (Coupling-loss Induced Quench) protection system.

The external dump resistor (acts like LR circuit) detects the quench electronically and it opens an external circuit breaker. In such way the current is forced to decay (it is dissipated) through the resistor.

Quench back heaters are in thermal contact with the winding (placed on the coils), they also detects the quench electronically. When a quench occurs, this heaters quenches other regions of the magnet by increasing the temperature, forcing the normal zone to grow more rapidly. With increasing the resistance the energy is dissipated.

After detecting quench, the CLIQ protection system introduces a high coupling loss, and hence heat, in the wire's copper matrix, resulting same effect as for quench heaters. This is done by introducing a series of fast oscillations in the transport current of the coils (13).

2.6 Magnet training

At their first powering, the magnets typically do not reach their designed limits. Therefore a process, named training, is need to reach the target values and to drive the magnets to their ultimate capabilities. During this process the mechanical structure will accommodate under the electromagnetic forces and the magnet will show better and better performance, continuously increasing the current level at quenching. The superconducting magnets also have a property named "memory". Training memory is evaluated after a thermal cycle: in a magnet with good memory after training and a successive thermal cycle, the first quench is not lower than the last of the previous training (see fig. 2.7a). If the magnets have good memory (i.e. the loss of training after a thermal cycle is low), they can be trained at a dedicated test station, and then installed into the LHC tunnel, such that they do not need to go through a long and costly training campaign after installation.

One of the key concepts in magnet training is the **load line**, which describes the evolution of the magnetic field in the material created by the current flowing through it (see fig.

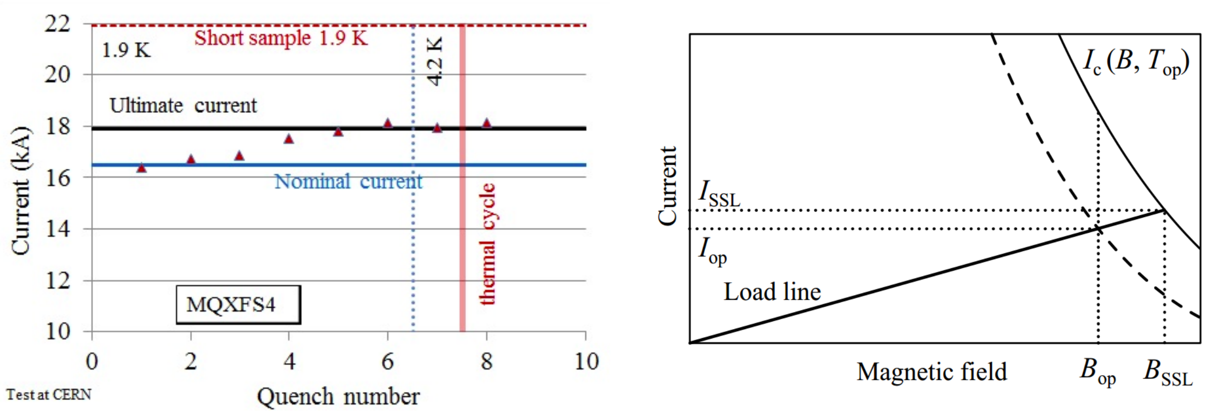

(a) Magnet training (9).

(b) Magnet load lines (14).

Figure 2.7: Superconducting magnet training curve and load lines.

2.7b). The so-called **short sample limit** (SSL) is the intersect of the load line and the critical current ($I_c(B, T_{op})$). The SSL indicates the theoretically calculated value of the maximum current which can flow in the magnet (14), and depends on the properties of the superconducting cable, which vary from magnet to magnet.

The nominal current (approx. 75-80% of short sample limit) is the target operation current of the magnets and the ultimate current ($\sim$ 8% more of nominal current) is the maximum allowed current for the magnets operating in the LHC. During testing of R&D magnets the current can go up until the short sample limit for experimental purposes, while for series magnets the allowed current is only the ultimate one.

Chapter 3

New technology Nb_3Sn accelerator magnets

The need of permanent innovations also influences the materials used for superconducting magnet productions. Comparing the properties of $NbTi$ and Nb_3Sn it is clear that the later one has better performance. The new inner triplet quadrupoles for the HL-LHC will be made from Nb_3Sn in order to provide the enough magnetic field gradient with larger aperture, while Nb_3Sn was already discovered in the 1950s, the technology for mass production was only developed in recent years. The main challenges of making magnets from Nb_3Sn is that the material is really brittle and winding of coils needs very delicate manipulation.

3.1 Coil production

Nb_3Sn is a ceramic, and as such it is very fragile in its structure. **Wires** made of Nb_3Sn cannot be bent, because they would break, therefore during winding the magnet coils, the Nb and Sn are in separated phases in the wires. The different processes used for making wires, containing separately the Sn and Nb, are the bronze process, internal Sn process or powder in tube (PIT).

The coils are then **heat treated** at $650 - 700\ °C$ in vacuum or inert gas (Ar) (15). During the heat treatment the Sn and Nb react to form the superconducting Nb_3Sn, at this point in the manufacturing process, the cable becomes brittle.

After the reaction the coils are **impregnated** in order to prevent motions. The coil is placed in an impregnation fixture in order to keep the coil in stable position. The fixture is inserted in a vacuum tank, evacuated the air and epoxy resin is injected. The epoxy has high viscosity at room temperature so it is heated to $60\ °C$ in order to cover uniformly the coil and then curing at $150\ °C$ to form a solid block (15). The surface of the coils is illustrated on figure 3.1 after the manufacturing phases. More detailed description of manufacturing accelerator magnets in articles (15), (16).

3.2 Focusing quadrupole magnets for HL-LHC

The Inner Triplet

As the name shows, the Inner Triplet (IT) contains three different magnets (or magnetic systems), which are focusing the particle beams consecutively in horizontal and vertical directions (see section 2.3). In total 8 inner triplets are in the tunnel, at both sides of the four main experiments. During the HL-LHC upgrade 4 of them will be replaced at the

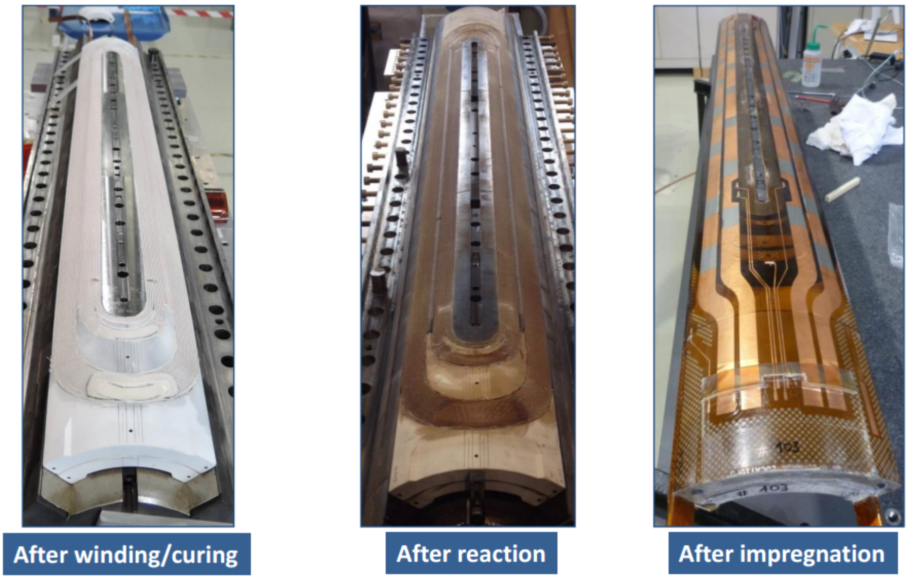

Figure 3.1: Nb_3Sn coil fabrication stages (11), (17). Winding the coil, when the Nb and Sn are in separated phases. Reaction on high temperatures, forming the superconducting Nb_3Sn material. Impregnation with epoxy to prevent coil motion.

ATLAS and CMS detectors. The new IT magnets will have Nb_3Sn superconducting coils, the cross-section presented on fig. 3.2. The current LHC and future (HL-LHC) layout of the Inner Triplet can be see on fig. 3.3.

The Inner Triplet is made of Q1, Q2 and Q3 magnets. The Q1 and Q3 magnet are MQXFA type, while Q2 is MQXFB type. The acronym MQXF is made from M - magnetic element, Q - quadrupole, X - interaction region (beams crossing), F - the 6^{th} inner triplet design. A and B magnet types are produced by different institutions, with slightly different design.

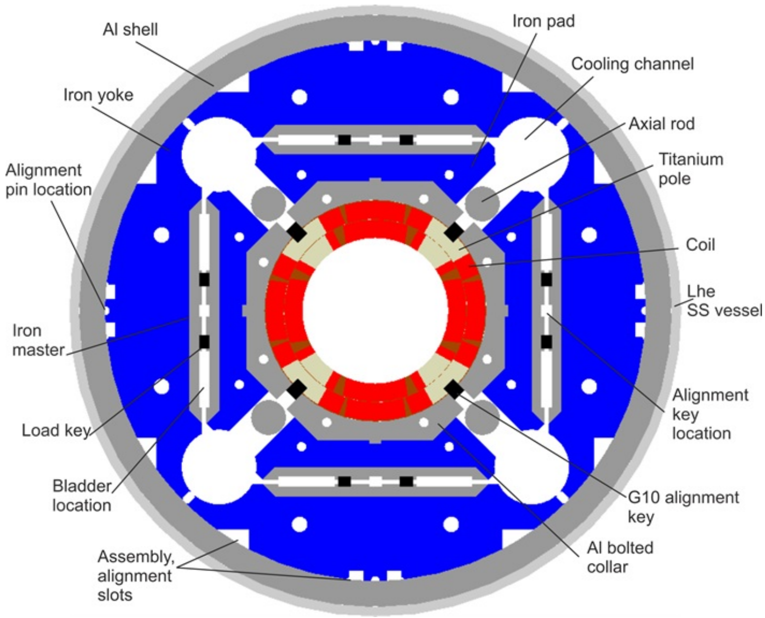

Figure 3.2: Cross-section of MQXF magnets (9).

According to the HL-LHC plans, the Q1 and Q3 will be consist from two magnets with 4.2 m length, assembled in the same cold mass and resulting 8.4 m magnetic length. These MQXFA type magnets are produced and tested in the US by the Accelerator Upgrade Project

(AUP). The Q2a and Q2b will be fabricated and tested at CERN with a magnetic length of 7.15 m, named MQXFB magnets. According to the described components, the Inner Triplet actually will be composed of 6 different magnets in total. The magnets will be made of Nb_3Sn superconducting coils, the aperture of the new quadrupoles will be 150 mm and they will have a nominal gradient of 132.6 T/m at nominal current 16.47 kA, and the nominal peak field reaches 11.4 T (1).

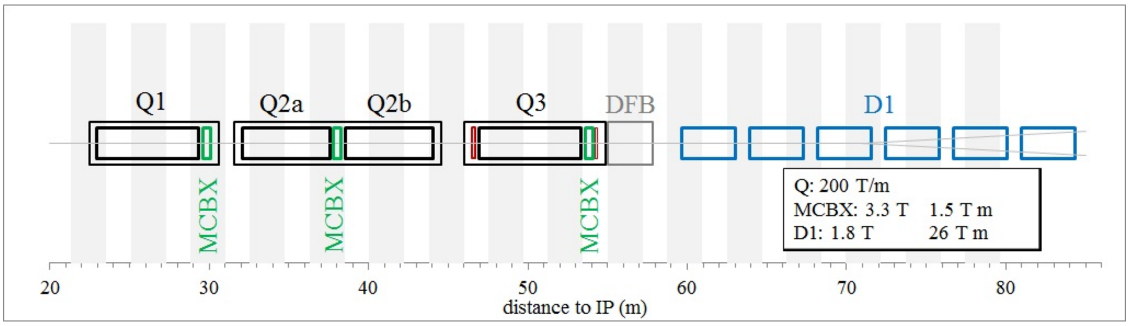

(a) The interaction region in the LHC.

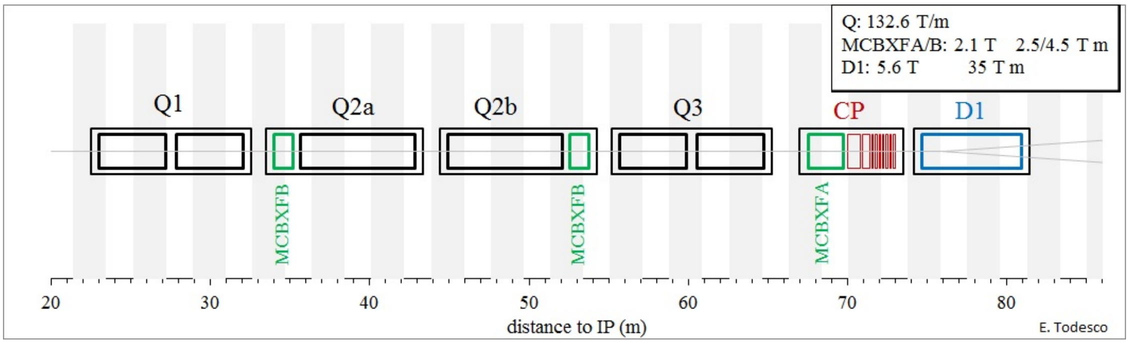

(b) The HL-LHC interaction region after upgrade.

Figure 3.3: Interaction region before and after the upgrade (9).

The **R&D process** of new magnets consists in many steps. It starts with making the magnets' design and then the first magnets, which are produced and tested, are the **short models**. As the name shows, the short model magnets have a reduced length, but they use the same technology and magnetic design as the new magnets. After the validation of the magnet design through the short models, the full length **prototype magnets** come in production and testing. Here the design is mostly finished and the focus is to assess if the manufacturing process needs to be improved or changed. The last step is the production and test of the **series magnets**, these magnets are not R&D but the actual magnets that will go to the LHC.

3.3 Quadrupole Nb_3Sn magnet short models - MQXFS

The MQXFS magnets are the short model version of the Inner Triplet magnets, which have the same diameter, magnetic design and manufacturing process as the series magnets, however they have reduced length. The parameters at cold powering (1.9 and 4.5 K) are described in table 3.1. The cross-section of the new quadrupole magnets (MQXF) is shown on figure 3.2.

Several short model magnets were already produced and tested for the HL-LHC upgrade. The magnets are nicknamed MQXFS followed by a number. The MQXFS1 were produced and tested in the US, the MQXFS-3,4,5,6 short models at CERN. Some magnets had changes in the mechanical structure and the modifications are represented by a letter following the magnet's name, e.g. MQXFS4c.

The coils of the MQXFS magnets are made from cables composed of 40 strands with a diameter of 0.85 mm. The coils are composed of 50 turns, wounded in 2 layers around a Ti-alloy pole. The layers are separated by ceramic binder. Before the impregnation quench heaters and voltage taps are placed on the top of the coils (15). The short model magnets weights approximately 2 tonnes, they are 2.1 m long with 0.614 m in diameter.

The mechanical design of the MQXF magnets is based on **bladder-key technology** (18). The preload of MQXF relies on this technology. Approximately half of the required azimuthal coil compression is applied at room temperature by inserting loading keys in between the iron masters, thus pressing collars against coils. The other part is gained after the cool-down, when the aluminium shell shrinks more than the iron and steel (19).

The detailed test results of the first short model MQXFS1 are described in articles (20), (21), further results and analysis for MQXFS3 and MQXFS5 in articles (21), (22). Test results MQXFS3c and MQXFS4 are summarized in (23). A very good summary on test results of the short models can be found in article (15), further analysis of the mechanical structure in (24) and (25).

Nominal Current	16.47 kA
Ultimate current	17.89 kA
Short sample limit	22 kA (1.9 K)
Nominal ramp rate	20 A/s
Nominal stored energy	1.5 MJ
Inductance (low current, nominal)	12 mH, 9 mH

Table 3.1: Cold powering parameters for MQXFS magnets.

Chapter 4

Magnet testing

After designing and fabricating a magnet a crucial point is also to test and validate it, confirming that it can be operated at the required parameters and giving good performance.

Once a magnet is designed the scientists need to have an appropriate test station which can be used for testing the magnet. This includes the designed size of a magnet (e.g. 1 m diameter, 3 m long), the required current level (even higher than 10 kA), the operation temperature (e.g. 1.9 K), etc. At the CERN's Magnet Test Facility - SM18 - the test stations are designed in such a way to be able to used not only for the present magnets, but to be adapted to future use. Making a test station, a compromise is needed between the possibilities ensured by the technology and the requirements for a new magnet test.

Magnet Test Facility (SM18)

The SM18 is the building, where most of the LHC and HL-LHC magnets are tested at cryogenic temperatures before being installed in the tunnel or for validation of magnets in R&D phase. The horizontal test benches were created to be able to host the testing of the 15-m-long dipole magnets and other cold masses for the LHC. The vertical stations are mainly used for shorter model magnet testing. For the tests of the MQXFS magnets the Cluster D and the HFM cryostats in the vertical station were used. These stations were constructed in such a way to be able to host the new magnet testing and also be able to host future larger and more powerful magnet tests. The parameters of the cryostats are described in table 4.1.

Properties	Cluster D	HFM
Diameter(m)	0.9	1.50
Length(m)	5.5	2.34
Volume(m^3)	3.5	4.13

Table 4.1: Properties of selected vertical test cryostats at SM18.

For reaching the required temperature a designed cryogenic system is used. The process of the cool-down has 3 stages:

- 300 - 80 K: cooling with saturated He gas, pre-cooled by liquid Nitrogen to 80 K
- 80 - 4.5 K: injecting liquid Helium (LHe)
- 4.5 - 1.9 K: pumping LHe in a heat exchanger in the cryostat

After the termination of the tests at low temperatures, the cryostat and the magnet will warm up gradually. During this process warm Helium is injected into the cryostat. Firstly Helium gas at 80 K is injected, after that controlled-temperature Helium gas (mix of 80 K and 300 K). Sometimes the temperature rises slowly, when the cryostat and the magnet are left in "passive" warm up.

4.1 Test plan

The purpose of R&D magnet testing is the validation of the design and exploring the magnet's behaviour in cryogenic conditions. Some of the test steps are done at both 4.5 K and 1.9 K temperature. In the case of series magnets, the test has the purpose to qualify the magnet, ensuring that is operates properly and it can be installed in the LHC.

The test plan contains the general verification processes and preparations, which ensure that the magnet is connected properly and well-protected; and test procedures.

The test plan contains:

- Preparation tests at warm - electrical insulation test, continuity
- Cooling down - RRR (residual resistivity ratio) measurement and temperature monitoring
- Cold powering preparation - electrical insulation test in LHe, CLIQ verification, energy extraction verification, quench heater verification
- Cold powering tests - training, quench analysis, ramp-rate studies, VI measurements, magnetic measurements
- Warming up - RRR measurement and temperature monitoring

During magnet training detailed quench analysis is done. Quench antennas and voltage taps are used in order to localize the place of transition to normal state and to analyze the quench propagation direction and velocity. For exploring the coils' properties and limits further tests are done.

Ramp-rate studies use different values of loading speed (increasing the current with e.g. 100 A/s or 200 A/s) for investigating which speed causes a premature quench. During VI measurements the current is increased gradually, having current plateaus at defined levels.

4.2 Data acquisition

Every test station has very complex instrumentation system. The cool-down and warm-up of the magnets is a supervised process with controlling the flow-rates, the temperature gradients etc. Temperature, flow and pressure sensors are placed in the cryostat and supporting systems and the magnet itself is also instrumented with many sensors. Voltage taps are placed on the conductors of the magnets in order to measure the voltage in the magnet. During operation, while the coils are in superconducting state, the measured voltage is the inductive voltage. When a quench starts to develop, a resistive voltage appears in the quenched region. These voltage signals can be used for quench detection and during post-processing for quench localization. Temperature sensors are placed outside of the magnets at different places (see section 4.2.2) in order to monitor the changes in temperature during thermal transients and testing. For measuring strain, at different parts of the magnets, electrical strain gauges (ESG) (26), (27) are used on the shell, pole, rods; for some magnets also optical strain gauges (FBG) (27) are placed on the poles, which are sensitive both to strain and temperature.

This thesis focuses on the MQXFS magnets and the evolution of stress during thermal transients inside the magnets. The strain and temperature sensors are handled by different departments and systems. In the case of the magnets the stress is calculated from the strain gauges, which are placed on the different part of the magnets.

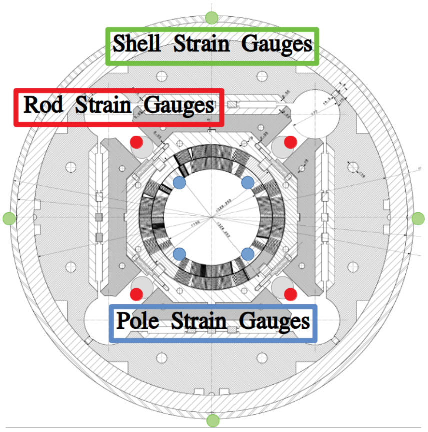

(a) The cross-section of MQXFS magnets and the location of strain gauges.

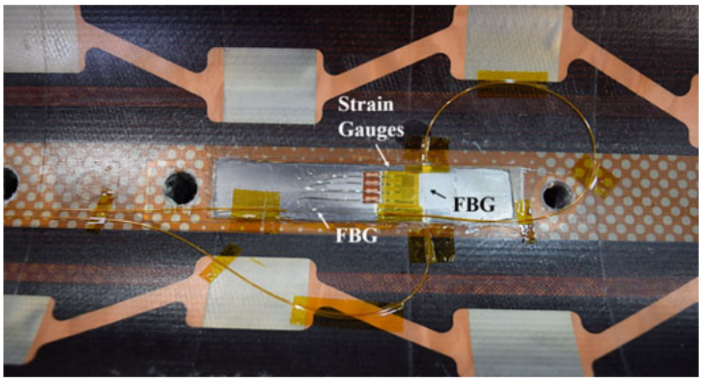

(b) Strain gauges placed on the poles (26), (27).

Figure 4.1: Strain gauges used for MQXFS magnets. The sensors are placed at the middle length of the magnets.

4.2.1 Strain gauges for stress analysis

The magnets are instrumented with strain gauges (28). The position of strain gauges can be seen on figure 4.1. The data acquisition system of strain measurements uses different frequency (sampling rate) of monitoring the data during the slow variation of values (e.g. during cool-down and warm-up) and a higher frequency in case of cold powering of the magnets to give more information in case of quench.

The operation of strain gauges is based on measuring voltage. From the measured voltage the resistance can be calculated and this resistance is proportional with the wire length. The deformation caused by thermal contraction or dilatation causes changes in the resistance of the wire, which can be observed in the voltage values. The change in resistivity is measured by a Wheatstone bridge. From the strain measurements the stress can be calculated as discussed in section 5.1.

The Gauge Factor is the sensitivity coefficient $GF = \frac{\Delta R}{RG \cdot \varepsilon}$, where ΔR is the change in the resistance caused due to strain, RG is the resistance of the undeformed gauge, and ε is the strain.

For strain measurement on the poles, thermal compensators (28) are used along with sensors placed on the poles. These compensators are placed on a piece of material same as the pole. The compensators' data should be subtracted from the strain gauge data on the coils. Their purpose is to separate the effect of the thermal contraction of the material from the strain in the material.

The strain gauges used for measurements in case of MQXFS6 magnet are: Cr-Ni/Polymide HBM, LC11-6/350 - shell, LC11-3/350 - rods, XC11-3/350 - coils (26), (27).

4.2.2 Temperature sensors

In case of every magnet 5 temperature sensors are placed on the shell at different positions. 2 on the bottom, 2 on the top and 1 at the middle of the magnet.

During the cool-down processes the cold helium gas/liquid is injected at the bottom part of the cryostats, resulting a temperature gradient along the magnet, therefore the bottom sensors will sense earlier the change in temperature. The temperature measured by sensors placed on the magnet shell could be different than what the magnet and the coils actually sense, due to radial gradients.

Between different stages of the cooling process in most of the cases there is a temperature plateau, when the temperature is held constant. If the plateau is long enough ($>$ 30 minutes), then the magnet should be at uniform temperature.

The strain gauges are placed at the middle length of the magnets, therefore for the analysis of strain and stress evolution by temperature, will be used the values measured by the middle temperature sensor. The temperature values are stored in the CALS database, from where the measurements can be requested at many sampling rates. For the analysis the 1 Hz rate is chosen, in order to be the same as for the strain gauges.

An example for cool-down process is shown on figure 4.2. It can be seen that the sensors at the bottom of the magnet show lower temperature than the others on top, the middle one has intermediate values. Also can be seen the stationary places (77 K and 4.5 K) between the cool-down stages, when the whole magnet is at the same temperature.

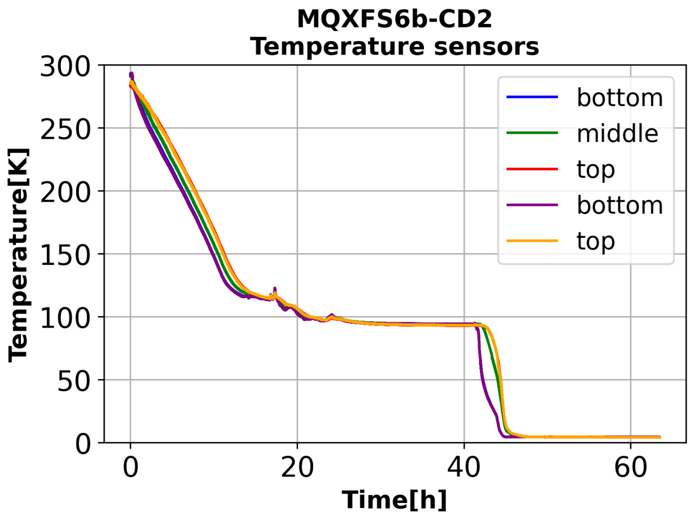

(a) Evolution of temperature.

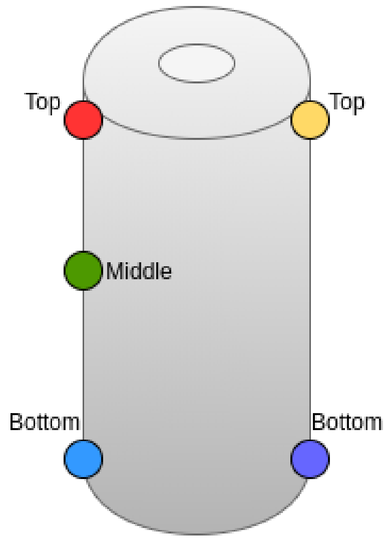

(b) The location of the temperature sensors.

Figure 4.2: Change of temperature by time during the second cool-down (CD2) of MQXFS6b magnet. The sensors on the bottom side of the magnet sense sooner the temperature decrements because the helium gas/liquid is injected on the bottom side of the cryostats.

Chapter 5

Study of strain and stress

As mentioned in the previous chapters, in the case of Nb_3Sn magnets the stress on the coils has a main influence on the magnet performance. During the thermal transient processes, like cool-down and warm-up, the magnet is exposed to large temperature variations, and the different components are not shrinking equally because they are made of different materials. The pressure on the coils increase during cool-down because the aluminium shell shrinks more than the inner structure. Stress values exceeding 150 - 200 MPa on the coils can cause irreversible damage on the magnet. In this study I will analyse the variation of stress during the thermal transients on MQXFS magnets. I will analyse both evolution by time and also representing the stress versus temperature.

As mentioned in section 4. the process to reach cryogenic conditions has 3 different stages: 300 - 80 K, 80 - 4.5 K and 4.5 - 1.9 K. During the cool-down process we can analyze the strain gauges data in 300 - 4.5 K range with 1 Hz sampling rate. This includes the first 2 steps of cooling. As the coefficient of thermal expansion is greatly reduced below $\sim$ 100 K, the largest changes in the stress of the magnet is expected in the first two phase of cool-down.

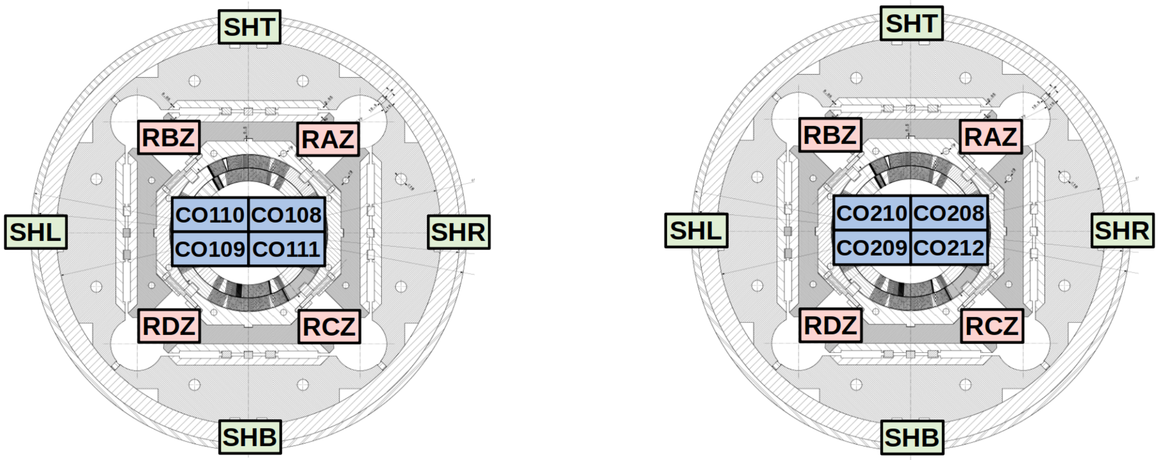

(a) MQXFS4a (b) MQXFS6b

Figure 5.1: Strain gauges name and location for MQXFS magnets indicated on the cross-section, the sensors are placed at the half-length of the magnets. The coil sensors are different, because they indicate the coil number.

The **temperature sensors** are placed on the outside of the magnet shell. Data is recorded from 5 temperature sensors: 2 at the bottom, 2 on the top, 1 at the middle length of the magnets.

The **strain gauges** are placed on the shell, rods and poles (between the coils). The exact places can be seen on fig. 5.1.

- 4 strain gauges on the shell, measuring strain both transverse (T) and longitudinal (Z) direction - they are named SH+place+direction e.g SHLT - shell strain gauge on left measuring in transverse direction. place=[bottom,left,top,right]
- 4 coil sensor placed on the poles (exception MQXFS4c - no coil strain sensors), measuring strain both transverse (T) and longitudinal (Z) direction, named CO + coil number + direction e.g $CO210\_T$.
- 4 rod strain sensors - one strain gauges on each rod, measuring strain only in longitudinal direction named RAZ, RBZ, RCZ, RDZ.

5.1 The matter of stress on magnet performance

For Nb_3Sn magnets the possible conductor degradation can happen at about 150-200 MPa on the coils. During cool-down the components shrink differently yielding a variation of coil stress. For preventing too high stress in the coils, it is very important to monitor the critical parameters during the tests and operation of the magnet. On the magnets the stress analysis can be done through mechanical measurements based on strain gauges, technical details in section 4.2.1.

Strain to stress transformation

Hooke's law for continuous media stays at the basis of strain measurements. Inside a continuous material the relationship between stress (σ) and strain (ε) can be given by a linear mathematical expression which is similar to Hooke's spring law. A solid medium can be compressed, stretched and sheared at the same time along different directions. So the stresses can be pushing, pulling and shearing. **Strain** means the deformation of dimensions per unit dimension (29).

This complexity is represented by two, second order tensors (29):

- strain tensor $\varepsilon = -s \cdot \sigma$, where s is the compliance tensor
- stress tensor $\sigma = -c \cdot \varepsilon$, where c is the stiffness/elasticity tensor

The stiffness tensor is a linear mapping between nine-nine numbers of stress and strain tensors, therefore is represented by a matrix of $3 \cdot 3 \cdot 3 \cdot 3 = 81$ numbers, c_{ijkl}. The relation between stress and strain:

$$\sigma_{ij} = -\sum_{k=1}^{3}\sum_{l=1}^{3} c_{ijkl}\varepsilon_{kl}, i, j = 1, 2, 3$$

The stress and strain tensors can be represented like:

$$\varepsilon = \begin{bmatrix} \varepsilon_{11} & \varepsilon_{12} & \varepsilon_{13} \\ \varepsilon_{21} & \varepsilon_{22} & \varepsilon_{23} \\ \varepsilon_{31} & \varepsilon_{32} & \varepsilon_{33} \end{bmatrix}, \sigma = \begin{bmatrix} \sigma_{11} & \sigma_{12} & \sigma_{13} \\ \sigma_{21} & \sigma_{22} & \sigma_{23} \\ \sigma_{31} & \sigma_{32} & \sigma_{33} \end{bmatrix}$$

The quantity which describes the expansion or contraction of a material in directions perpendicular to the loading direction is called **Poisson's ratio** (ν), and it is material dependent.

An other important property is the **Young's modulus**, which measures the stiffness of a solid material. The Young's modulus (E) defines the relationship between stress and strain of an uniaxial deformation.

Tensional stress of uniform bar

A rod of any elastic material may be viewed as a linear spring. The rod has length L and cross-sectional area A. Its tensile stress σ is linearly proportional to its fractional extension or strain ε multiplied by the modulus of elasticity E (29). It is analogous to the original Hooke's springs law replacing F-force with σ - stress, x - elongation with ε - strain and k - stiffness with E - Young's modulus, resulting $\sigma = E\varepsilon$.

Isotropic materials

For isotropic media (which have the same physical properties in any direction), the stiffness tensor c can be reduced to only two independent numbers, **the bulk modulus K** and the **shear modulus G**, that quantify the material's resistance to changes in volume and to shearing deformations, respectively.

$$\varepsilon_{ij} = \big(\frac{1}{3}\varepsilon_{kk}\delta_{ij}\big) + \big(\varepsilon_{ij} - \frac{1}{3}\varepsilon_{kk}\delta_{ij}\big) \tag{5.1}$$

General form of Hooke's law for isotropic materials (29):

$$\sigma_{ij} = 3K\big(\frac{1}{3}\varepsilon_{kk}\delta_{ij}\big) + 2G\big(\varepsilon_{ij} - \frac{1}{3}\varepsilon_{kk}\delta_{ij}\big) \tag{5.2}$$

, $K = \frac{E}{3(1-2\nu)}$ is and $G = \frac{E}{2(1+\nu)}$.

In terms of Young's modulus and Poisson's ratio, the general form of stress for isotropic materials (29):

$$\varepsilon_{ij} = \frac{1}{E}(\sigma_{ij} - \nu(\sigma_{kk}\delta_{ij} - \sigma_{ij})) \tag{5.3}$$

Expanded form:

$$\begin{aligned} \varepsilon_{11} &= \frac{1}{E}\big(\sigma_{11} - \nu(\sigma_{22} + \sigma_{33})\big) \\ \varepsilon_{22} &= \frac{1}{E}\big(\sigma_{22} - \nu(\sigma_{11} + \sigma_{33})\big) \\ \varepsilon_{33} &= \frac{1}{E}\big(\sigma_{33} - \nu(\sigma_{11} + \sigma_{22})\big) \\ \varepsilon_{12} = \frac{1}{2G}\sigma_{12}; \varepsilon_{13} &= \frac{1}{2G}\sigma_{13}; \varepsilon_{23} = \frac{1}{2G}\sigma_{23} \end{aligned} \tag{5.4}$$

Plane stress

In the case of the plane stress the values in the 3^{rd} direction are considered to be negligible, therefore $\sigma_{31} = \sigma_{13} = \sigma_{32} = \sigma_{23} = \sigma_{33} = 0$. The simplified relationship for an isotropic materials becomes (29):

$$\begin{bmatrix} \sigma_{11} \\ \sigma_{22} \\ \sigma_{12} \end{bmatrix} = \frac{E}{1-\nu^2} \begin{bmatrix} 1 & \nu & 0 \\ \nu & 1 & 0 \\ 0 & 0 & \frac{1-\nu}{2} \end{bmatrix} \begin{bmatrix} \varepsilon_{11} \\ \varepsilon_{22} \\ 2\varepsilon_{12} \end{bmatrix} \tag{5.5}$$

Final equations

The stress could not be explicitly measured on the components of the MQXF magnets. For calculating the stress inside the magnets, strain gauges are placed on the different parts of the magnets. From the measured strain values the stress level can be deduced.

Strain gauges are placed on the coils, shell and rods in most cases. The strain sensors can measure longitudinal and transversal components of the strain.

The **rods** can be viewed as a linear spring, therefore the stress will be:

$$\sigma = E\varepsilon \tag{5.6}$$

, where σ is the stress, ε is the strain and E is the Young's modulus of the material.

For **shell** and **coils** stress calculations we assume that we have plane stress, using notations:
$\sigma_{11} = \sigma_T, \varepsilon_{11} = \varepsilon_T$, for transversal direction and
$\sigma_{22} = \sigma_Z, \varepsilon_{22} = \varepsilon_Z$, for longitudinal direction.

Therefore the formulas for calculating the stress in case of the shell and the coils in different directions from equation 5.5 became (30):

$$\sigma_T = \frac{E}{1-\nu^2}(\varepsilon_T + \nu \cdot \varepsilon_Z) \tag{5.7}$$

$$\sigma_Z = \frac{E}{1-\nu^2}(\varepsilon_Z + \nu \cdot \varepsilon_T) \tag{5.8}$$

, where ν is the Poisson ratio of the material.

5.2 Young's modulus and cryogenic compensation

As mentioned in section 5.1 the stress is proportional with the Young's modulus, which could have also a temperature dependence. Further I will describe my method for determining the Young's modulus at the different temperature values. A cryogenic compensation is also applied for the strain measurements.

Young's modulus

In case of aluminium, from which the rods and shell of the magnet are produced, the Young's modulus has a temperature dependence. According to the mechanical measurements team, for the calculations two values of E of aluminium alloy is fixed: 70 GPa at room temperature, and 79 GPa at 77 K and below (31). For the Poisson ratio, which is in the equation 5.7 and 5.8, $\nu = 0.34$ is used (31). The coil sensor are not placed on the coils itself but on the titanium structure. For the titanium alloy the Poisson ratio $\nu = 0.3$ and $E = 130$ GPa in the whole temperature range (31).

In order to get more appropriate result for the thermal transient phase when the temperature is changing, we should pay attention also to the more detailed change in Young's modulus. The aluminium alloy 7175 is used for the shell and rods of the magnets. However we do not have the exact values for this type of aluminium, but there are measurements for Al 6061 and 5083 (32). The temperature dependence of the Young's modulus is illustrated on the figure 5.2a, it contains the two reference aluminium alloy Young's modulus and a third one deducted from those to meet our preferences E(300K) = 70 GPa and E(4.5K) =

79 GPa. In order to determine the Young's modulus for each temperature value I used 4^{th} grade polynomial function like equation 5.9.

$$E(T) = 79.27 + 5.7 \cdot 10^{-3} \cdot T - 3 \cdot 10^{-4} \cdot T^2 + 9.548 \cdot 10^{-7} \cdot T^3 - 1.09 \cdot 10^{-9} \cdot T^4 \quad (5.9)$$

Cryogenic compensation

The strain gauges have a limited sensitivity - k (28), which is also influenced by the temperature, 4 point is fixed for the k factor in the table 5.1.

T[K]	1.9	4.2	77	300
k	0.92	0.92	0.935	1

Table 5.1: Fixed values for cryogenic compensation - k values at specific temperatures (28).

For determining the k factor on whole range of temperature I used second order polynomial approximation eq. 5.10, with this factor the raw data from the all strain gauges needs to be multiplied.

$$k(T) = 0.9195 + 1.78 \cdot 10^{-4} \cdot T + 3 \cdot 10^{-7} \cdot T^2 \quad (5.10)$$

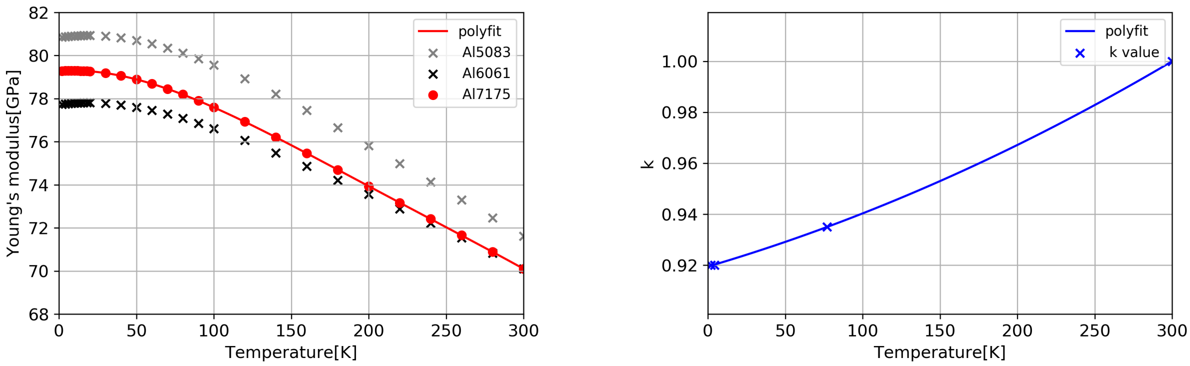

(a) Young's modulus for aluminium alloys. (b) Strain gauges sensitivity - k

Figure 5.2: Approximation for Young's modulus and k factor.

5.3 Data analysis process

Synchronization

The temperature and strain values are stored in different files recorded by different systems. As first step these data should be synchronized, which means that we have the same timing for both temperature sensors and strain gauges. As sometimes data is lost (e.g. due to power cuts), synchronizing the start of the temperature and strain files is not enough. To tackle these cases, we assume that the change in temperature will cause immediate change in strain values. An example for right timing for the temperature and strain gauges is shown on figure 5.3a . Also the sampling rate of the measurements has to be identical - in our case is 1 Hz.

Data manipulation

After selecting the right data from temperature and strain files, the next step is to manage the signal losses, and filter out the noise. Every measurement is unique and needs to be manipulated individually. For example during power cuts the strain sensor had signal losses but the temperature was recorded continuously. For this situation the gap for strain values should be replaced with no-values or interpolated, when there was no variation identified in temperature.

There were also systematical spikes in temperature values caused by the switch between the calibration ranges of the sensors, resulting spike in temperature, however the real temperature was not changed. For cryostat in cluster D the spikes were around 40 K for HFM around 70 and 6 K. These spikes were also eliminated.

In some of the cases the coil strain measurements had 2 channel: one channel for the strain gauge on the wedge and an other one for the compensator which was placed on a little piece of material. When we have these two values separately then the compensator's values should be subtracted from the strain values on coil wedge. More info in section 4.2.1.

The calibration factor k is also applied on the measured strain values, according to equation 5.10.

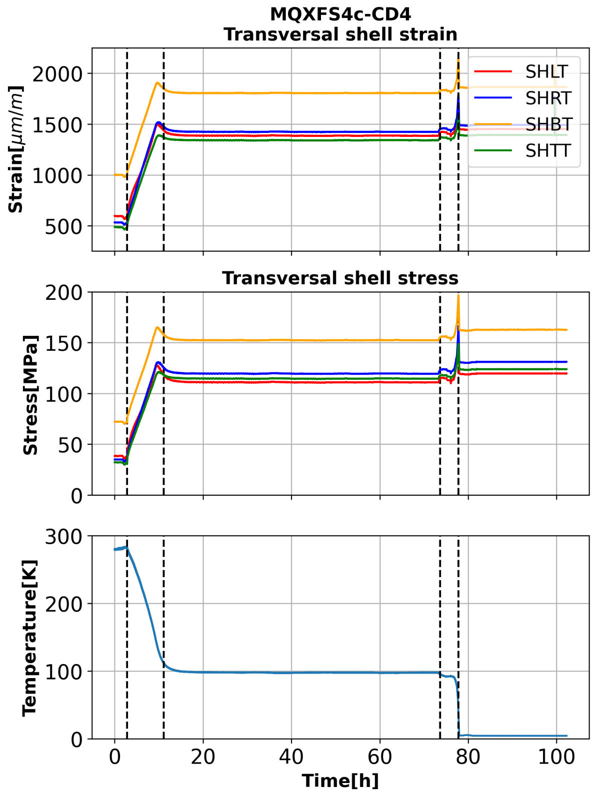

(a) Cooling

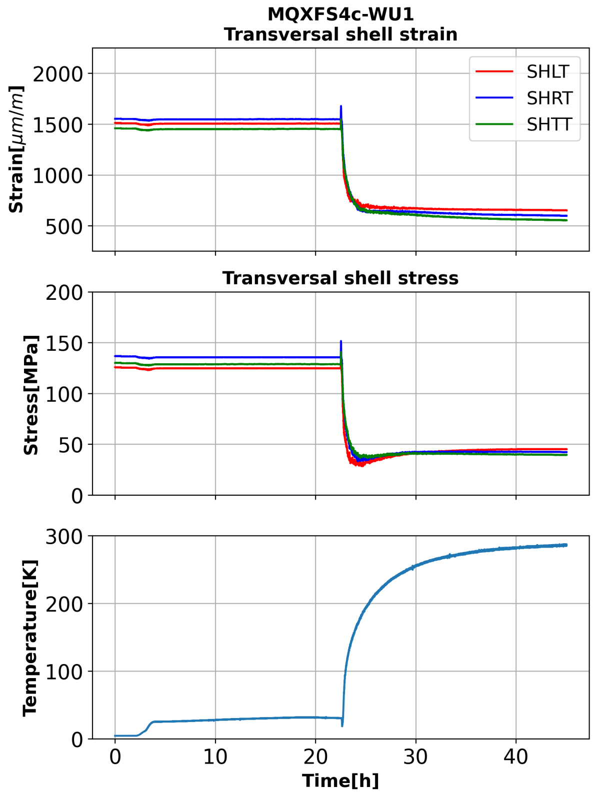

(b) Warming

Figure 5.3: Shell strain and stress value evolution in time during cool-down and warm-up. As the temperature is decreasing, the stress will grow inside the magnet. Synchronized strain and temperature measurements: the change in temperature causes change in strain measurements simultaneously.

Calculating stress from strain

The next step is to calculate the stress from the strain measurements using equations 5.7 and 5.8 mentioned already in section 5.1, therefore the stress for rods $\sigma = \varepsilon E$ and for shell and poles $\sigma_{T,Z} = \frac{E}{1-\nu^2}(\varepsilon_{T,Z} + \nu \cdot \varepsilon_{Z,T})$.

The strain and stress evolution in time is shown on fig. 5.3 for the magnet shell. During cool-down an increment in stress can be observed when the temperature goes down. Fast changes are seen at the start of the different cool-down phases. In the case of warming, on the fig. 5.3b, can be seen that as soon as the temperature starts to increase rapidly, the stress values are decreasing, because the aluminium shell and the cold mass will broaden.

Temperature dependence of stress

After filtering and conditioning temperature and strain/stress measurements and they are also synchronized, the strain/stress values can be plotted in the function of the temperature.

On the figures is clearly noticeable that the stress will increase by decreasing of the temperature. This is due to the shrinkage of the aluminium shell and rods, which contributes to the increment of the stress inside the magnet. This trend can be observed in values measured both on the rods (fig. 5.4) and on the shell (fig. 5.5). A smooth increase can be seen during 300 - 80 K in stress (decrease for warming 80 - 300 K), while peaks appear at the start of some cool-down and warm-up phases.

The shape of the stress evolution lines is obviously different for the cool-downs and warm-ups in case of the shell, while for the rods the trend is very similar. During the cool-downs in every case we can see a peak in each step of the cool-down, while during warm-up such kind of variations are not observable. During thermal cycles (consecutive cool-down and warm-up) the mechanical structure of the magnet can have differences at the start and end point of strain/stress values due to the accommodation of the mechanical structure.

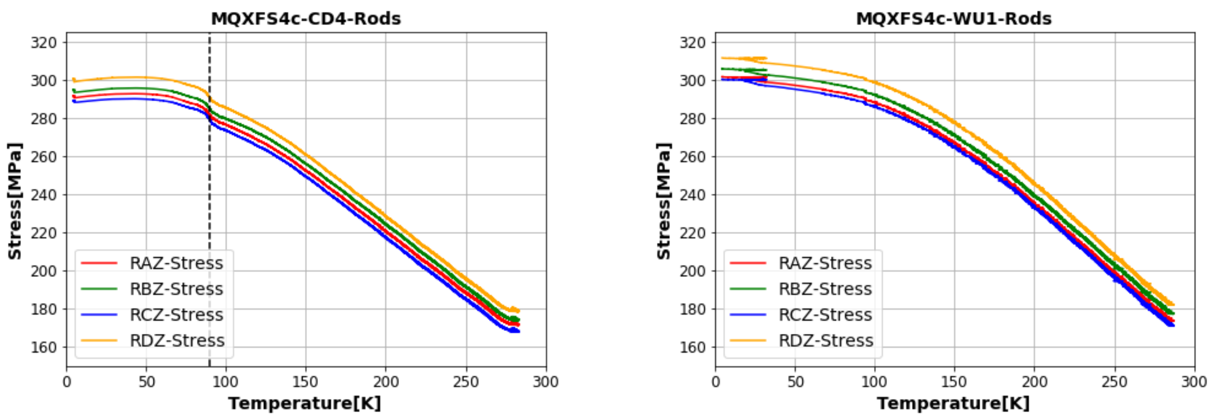

(a) Cooling (b) Warming

Figure 5.4: Stress values for rods during thermal transients. The results show very similar trend in case of cool-downs and warm-ups. The different values at low temperature maybe caused by the accommodation of the mechanical structure of the magnet by time.

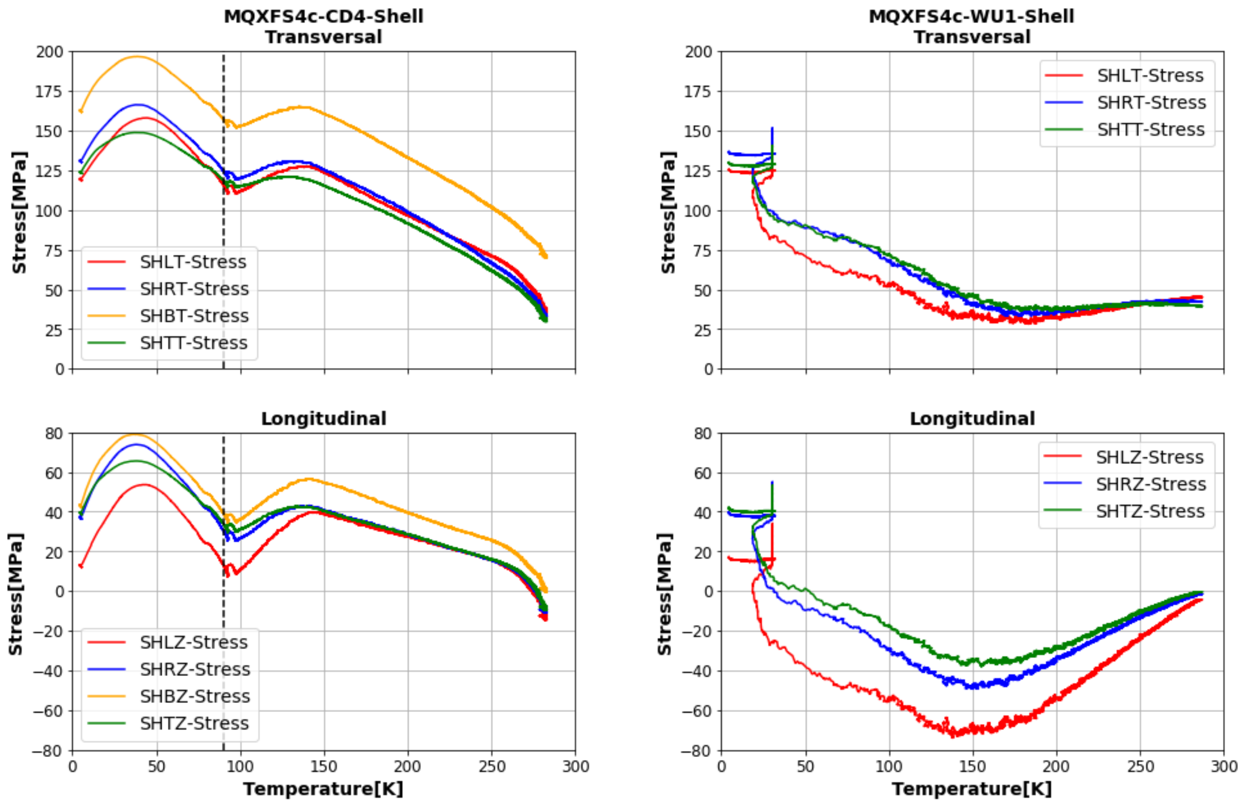

(a) Cooling (b) Warming

Figure 5.5: Stress values for shell during thermal transients, both longitudinal and transverse direction. The two stages of cool-down can be identified, separating the plot in two part. From 300 to approx. 80 K the cooling with Helium gas, after that cooling with liquid He.

Chapter 6

Magnet test analysis and discussion

The short models tested during my practical stage at CERN were the MQXFS4c and MQXFS6b. The individual test results per magnet are discussed in this chapter. In addition a comparison with the previous test results will be done - for different assemblies. The influences of cooling rate, temperature gradient and cryostat shape are also analysed.

The **MQXFS4** magnet was assembled three times, the modification in the mechanical structure were noted by MQXFS4a, MQXFS4b and MQXFS4c. The coils for MQXFS4 magnets were made of conductors produced by restack rod process (RRP) method. The magnet coils and most of the structure were unchanged, and the target pre-stress levels were kept constant. The last model, MQXFS4c was cooled down and warmed up six times. The strain gauges measurements are missing for the 5^{th} cool-down and 4^{th} warm-up. The MQXFS4a and MQXFS4c were tested in the cryostat in Cluster D, while MQXFS4b in the HFM cryostat. In the case of MQXFS4b and MQXFS4c the pole strain gauges were removed.

The **MQXFS6** had two different assemblies: MQXFS6a and MQXFS6b, both tested in HFM cryostat. The coils of MQXFS6 magnets are made from PIT (powder in tube) conductors. Two coils were replaced during the change, with coils from the MQXFS5 model. The MQXFS6b had 4 cool-downs and 4 warm-ups. The strain gauges measurements are missing for the third cool-down and second warm-up.

Details about the number of thermal transients and the testing cryostats for all of the MQXFS4 and MQXFS6 magnets are described in table 6.1.

Short model	MQXFS4			MQXFS6	
Assembly	a	b	c	a	b
Cryostat	D	HFM	D	HFM	HFM
Nr. of thermal transients	4	2	12	2	8

Table 6.1: Number of thermal transients (cool-downs and warm-ups) for MQXFS4 and MQXFS6 magnets and the test cryostat, where the magnets were tested.

The temperature dependence of the stress will be presented below during cool-downs and warm-ups for the two short model magnet. The analysis is done separately on the rods, the shell and the coils. On the figures below the averaged values are presented for the stress values transformed from the strain measurements.

6.1 Test results for MQXFS4 and MQXFS6

Rods

The temperature dependence of stress measured on the rods in longitudinal direction is illustrated on fig. 6.1 for both MQXFS4 and MQXFS6 magnet assemblies. The shape of the curves is similar in the case of the thermal transients: cool-down and warm-up. The stress at room temperature is around 170 MPa, while at cold it is increased to approximately 300 MPa following a monoton evolution. A very small change can be identified in the lines around 80 K, when the injection of liquid Helium starts. The absolute change in stress caused by the cool-down is approximately 130 MPa. The stress analysis on rods remains consistent for all MQXFS4 and MQXFS6 magnets, the thermal transients are very similar and they also overlap as can be seen on figure 6.1.

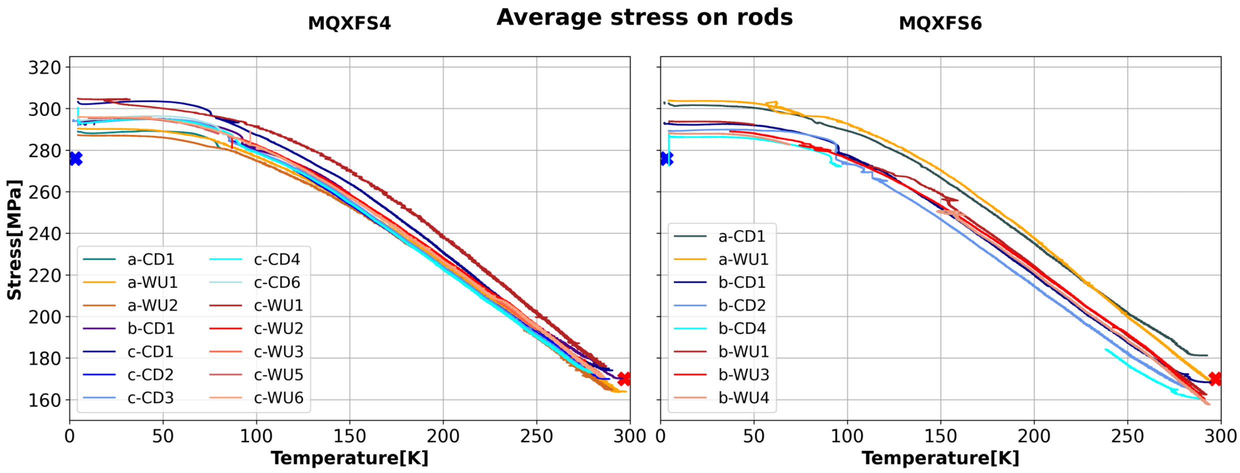

Figure 6.1: Stress values on the rods in function of temperature for MQXFS4 and MQXFS6 magnets during thermal transients (marked with bluish and reddish colors in case of cool-down and warm-up respectively - the blue and red crosses mark the target values). The stress has very consistent behaviour during thermal transients.

Shell

The temperature dependence of stress measured on the shell in longitudinal and transverse direction is illustrated on fig. 6.2 for the magnets. The evolution lines have different shape for the thermal transients, during cool-down they have upper flexion, while during warm-up it is inverse.

In the case of MQXFS4c, the difference in shell stress measured at room temperature and at cold is roughly 75 MPa in transverse and 20 MPa in longitudinal direction. During cool-downs the two steps of cooling (300 - 80 K with cold gaseous helium, and 80 - 4.5 K with liquid helium) can be easily identified: a peak can be observed during both stages.

For MQXFS6b the absolute change is smaller in the stress values for transverse direction. The difference between stress values measured at warm and cold is 50 MPa in transverse and 20 MPa in longitudinal direction. The smaller value related to MQXFS4c for transverse direction can be caused by the different level of pre-load during assembly.

A big difference in the shape of the curves can be identified in temperature range of 80 - 4.5 K, when the liquid Helium is injected. For the magnets tested in HFM cryostat such as MQXFS6a, MQXFS6b and MQXFS4b, the curve is flatten in this range. The MQXFS4c was tested in cryostat at Cluster D, and shows a second stress peak in this range.

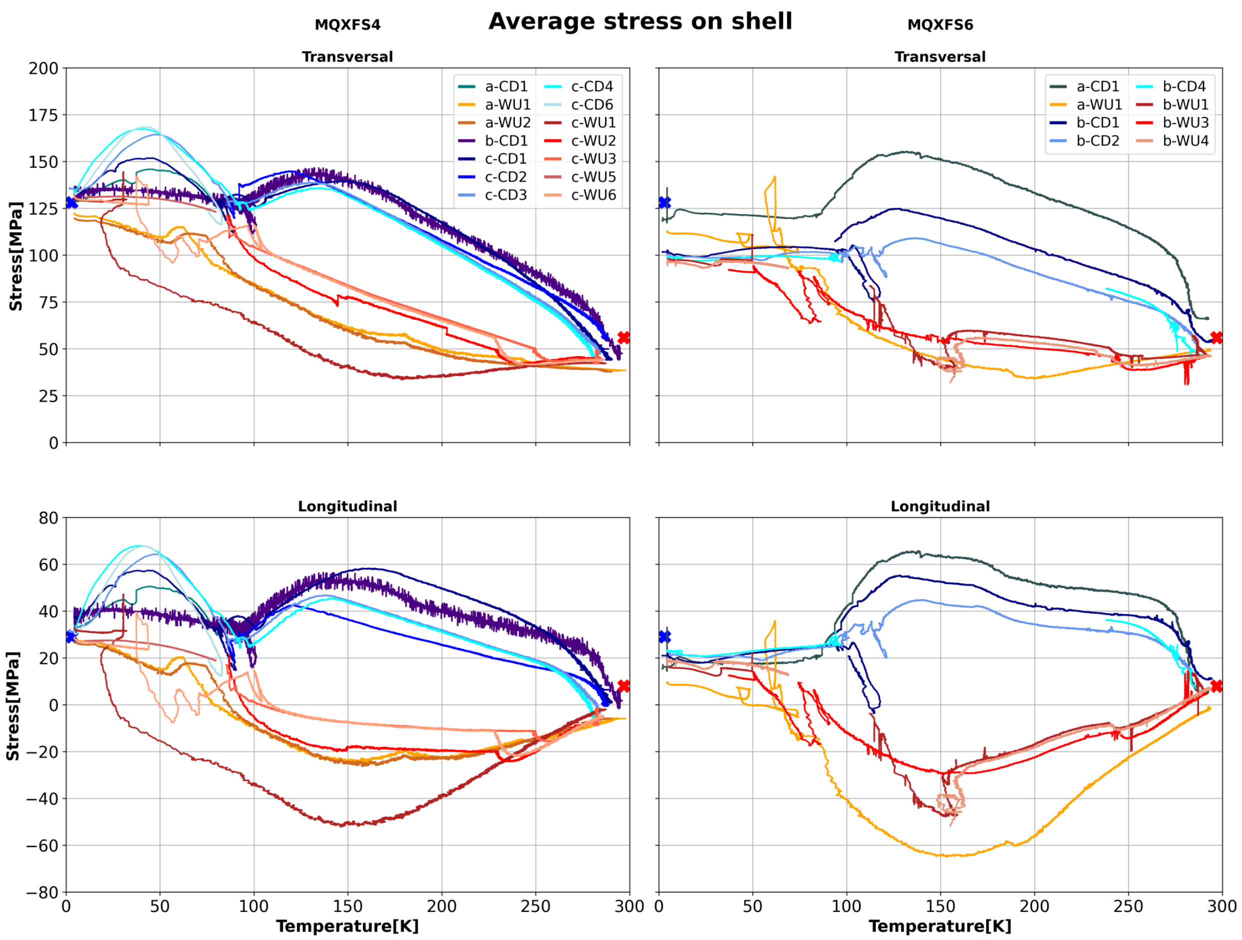

Figure 6.2: Stress on the shell in function of temperature for MQXFS4 and MQXFS6 magnets during thermal transients. The difference between cool-downs and warm-ups can be seen in the flexion of the curves. The target values are marked with blue and red crosses at cold and warm. For MQXFS6 the curves are flattened in the range on 80 - 4.5 K.

These stress peaks could be caused by the cool-down process, or could be measurement artifacts. For example the temperature sensors are cooling faster than the shell itself and the values should be delayed in time. The delay can also be caused by the strain gauge compensator which is placed on the separated piece of material, while the shell mass much larger. This will be discussed further.

Coils

The stress levels on the coils (poles) are shown on figure 6.3. The strain gauges were removed in the case of MQXFS4b-c, there are no direct measurements on the coils. In order to obtain an estimation of which shell stress levels are appropriate we can use the previous measurements in which the coil stress was also adequate. In the following cool-downs/warm-ups, if the shell stress is the same then the coil stress should be the also the same.

The change in the stress on the coils during thermal transients is smaller than on the shell. In transverse direction the change is around 10 MPa, while in longitudinal direction is 40 MPa for MQXFS6b. During warm-ups the curves have larger amplitude than in the case of cool-downs. The critical stress values 150 MPa on the coils is not exceeded in none of the cases.

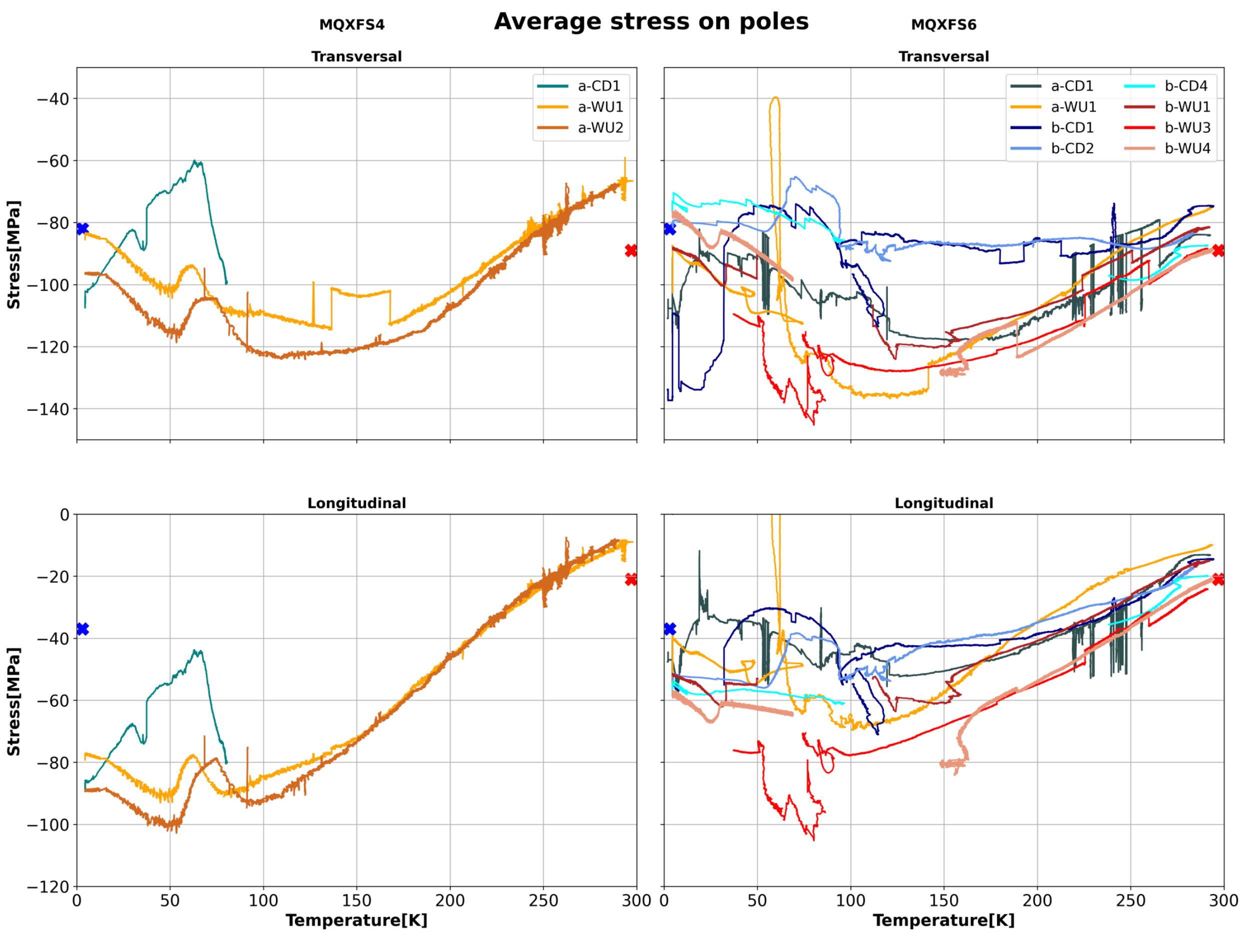

Figure 6.3: Stress values measured on the poles (coils) for the thermal transient of MQXFS4a and MQXFS6 magnet assemblies. The target values are marked with blue and red crosses at cold and warm. The critical stress value (150 MPa) is not exceeded during transients.

6.2 Comparison with target values

The target values, based on finite element modelling (19), for the stress level on the magnets are marked by the blue and red crosses at room temperature and at cold on fig. 6.1, 6.2 and 6.3. The measured values are approaching the designed values very well in most of the cases. In the case of the shell and coils the values are not changing uniformly during the transient periods, but the values after the transients, when the magnet is in thermal equilibrium state (the temperature of the magnet is uniform), are in good agreement with the predictions.

The target values (31) at cold and room-temperature for the different parts of the magnet are summarized in table 6.2.

Temperature	Stress[MPa]				
	Rod	ShellT	ShellZ	CoilT	CoilZ
warm	170	56	8	-89	-21
cold	276	128	29	-82	-37

Table 6.2: Target values of stress at warm and cold temperatures for MQXFS4 and MQXFS6 magnets.

6.3 Influence of mechanical properties of the cryostats

As mentioned before, for the magnets tested in the HFM cryostat the stress vs. temperature evolutions are more flat than in the case of magnets tested in Cluster D in the 80 - 4.5 K range. In spite of that in the range of 300 - 80 K the evolution of stress is similar in the case of both cryostat.

The HFM and Cluster D stations both have the same method for the cooling step 80 - 4.5 K, it is done with liquid helium, which evaporates when reaching the bottom of the cryostat, and exits the cryostat at the top.

The Cluster D is narrower, so the space for helium gas to flow is very small ($\sim$ 12 cm): helium gas flow is very fast (compared to HFM, where space for the flow is $\sim$ 40 cm), meaning a better thermal exchange. As a consequence, the sensors (which are on the magnet shell) cool-down faster in Cluster D. So most probably it's an artifact caused by the different temperature of the strain sensors (in the magnet and compensator). This fact can cause a change in the flow of the liquid Helium and also can influence the shape of the curves in the second step of cool-down.

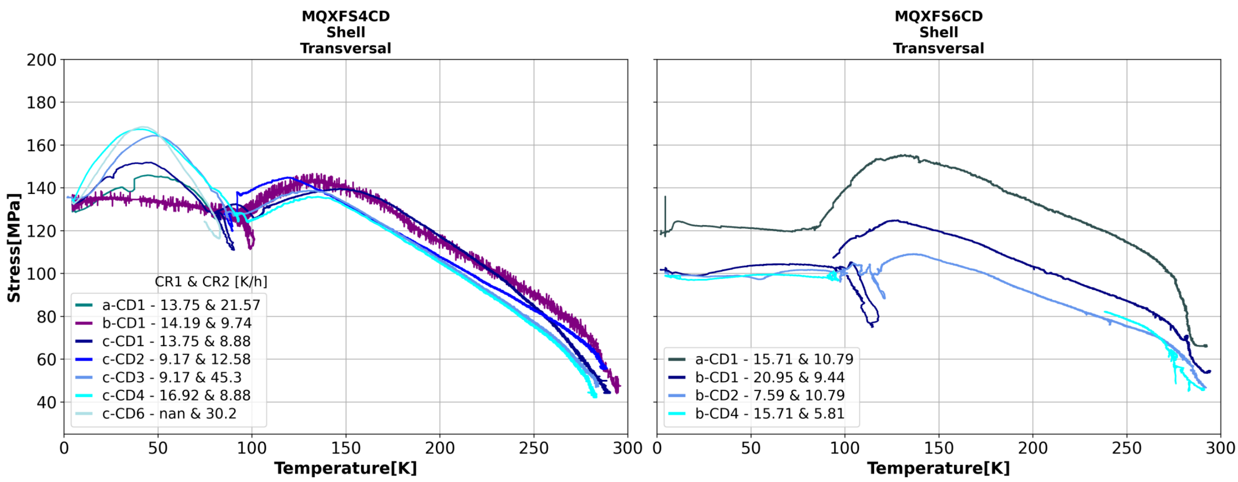

Figure 6.4: Temperature dependence of shell transversal stress during cool-down of MQXFS4 and MQXFS6 magnets. The cooling rates in range 300-80 K (CR1) and 80 - 4.5 K (CR2) are measured in K/h. The MQXFS4b and all MQXFS6 assemblies were tested in HFM, while the MQXFS4a,c in Cluster D.

6.4 Influence of cooling rates

The cooling rates for the two different steps of cooling are marked on the plots in K/h units, the exact values are shown on fig 6.4. In the case of the shell stress analysis these two cooling steps can be easily identified, however there was no relation found between the amplitude of the peaks an the speed of cooling during the analysis. For example on figure 6.4 in range 90 - 4.5 K the maximum peak is for the fourth cool-down of the MQXFS4c. The cooling rate was 8.88 K/h for that cool-down, however the rate was 45.3 K/h during the third cool-down, still that peak is not the largest one. In conclusion the cooling rate does not influence the stress evolution inside the magnets.

The displacements of the stress levels can be rather explained by existence of training and change in the mechanical structure more than the values of the cooling rates. For example after the first training of MQXFS6b, the stress lines got lower as can be seen also in the case of the shell fig. 6.4.

6.5 Influence of temperature differences

As mentioned before, the magnets start to cool-down from bottom to top direction. This results in a temperature gradient along the magnet. The bottom part of the magnet will cool down faster. The maximum differences in temperature measured on the top and bottom part of the magnets are shown on fig. 6.6, where also the cooling rates are presented in the case of the cool-downs. There was no dependence identified between value of stress level evolution shape and temperature differences.

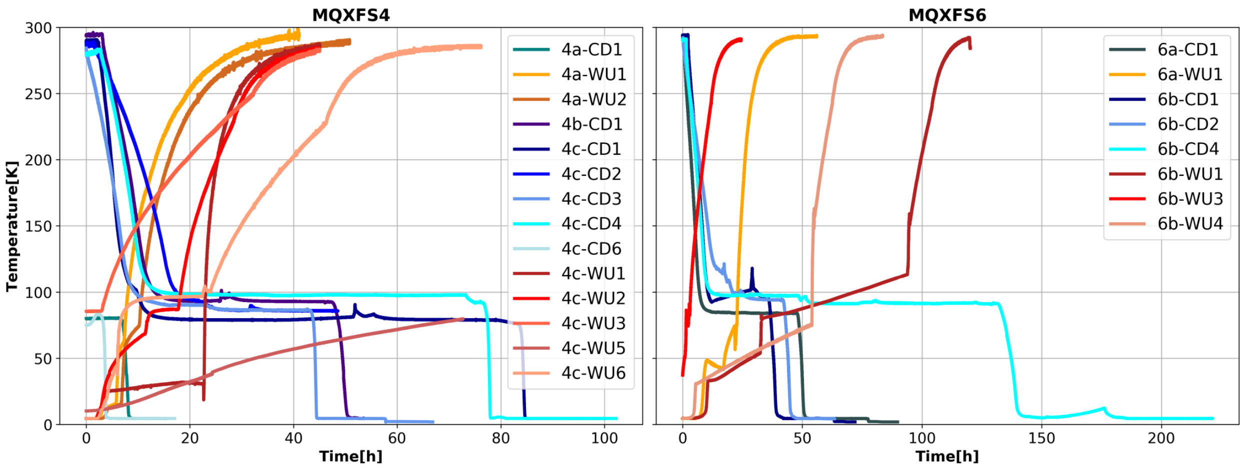

Figure 6.5: Evolution of the temperature during thermal transients (cooling with gas/liquid Helium, warming with Helium gas at controlled temperatures). The fifth warm-up of MQXFS4c (WU5) was special, letting the magnet to warm "passively" (without using Helium gas).

In the case of MQXFS4c the fifth warm-up was really special. There was no warm Helium gas injected into the cryostat, therefore the magnet was warming passively. The variation in temperature can be seen on fig. 6.5, a 80 K rise in temperature was achieved in approximately 3 days. On the figure 6.2, where the shell stress is plotted, can be seen that the fifth warm-up of MQXFS4c has also different trend compared to the other warm-up lines, therefore we can consider this warm-up as quasi-static.

The stress values on the coils (poles) for all the tested MQXFS4 and MQXFS6 magnets are presented on fig. 6.3. The images show that the critical stress of 150 MPa is never exceeded, which means that the magnet coils were not degraded during the thermal transients. This analysis validates that the testing circumstances of the magnets are suitable. If the flow rates are maintained in the same range and the thermal gradient does not exceed the 50 K in the magnets at the first step of cooling (300 - 80 K), then the superconducting coil will not be damaged.

During cool-downs the cooling rates generally range between 7 - 21 K/h in the first step of cooling, when saturated Helium gas is used. In this step the maximum temperature differences along the magnet (between top and bottom part) had values 25 - 50 K. After the first cooling step the temperature values are around 77 - 90 K. The next cooling step is the injection of liquid Helium ($\sim$ 4.5 K) at the bottom of the cryostat. During this step the cooling rates were recorded in 5 - 46 K/h interval. The maximum temperature difference (top-bottom) can reach 80 K along the magnet caused by the difference in the temperature of liquid Helium at the bottom and the gaseous Helium at the top of the cryostat.

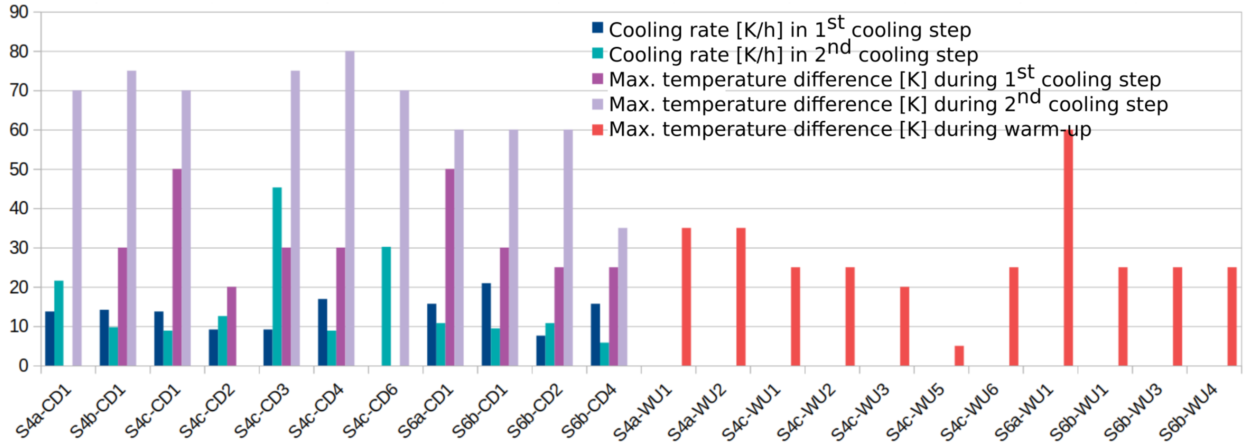

Figure 6.6: Cooling rates and maximum temperature differences along the MQXFS magnets recorded during thermal transients (cool-downs and warm-ups).

In the case of warm-ups controlled temperature gaseous Helium is injected to the cryostat. In special cases the magnet can warm up passively (no Helium gas injection). During warm-up temperature differences were averaged 25 - 35 K along the magnets. A minimum 5 K difference was measured in the case of MQXFS4c magnet during fifth warm-up, when the magnet was left to warm-up passively.

Conclusions

The world largest particle accelerator at CERN is before a big upgrade. The aim of the HL-LHC project is to increase the luminosity of the machine. The luminosity is proportional with the number of collisions per second, higher luminosity means more data to analyse for the researchers. The luminosity is influenced by many factors, therefore during the upgrade many departments need to collaborate and develop the machine. One way to increase the luminosity is to reduce the cross-section of the particle beam, another possibility is to collect more particles after the collision points. Combining these two factors the density of the particle will increase and more collisions can take place at the detectors. This can be achieved by, among other upgrades, replacing the focusing magnets before and after the experiments. The new focusing magnets for the HL-HLC project, the MQXF magnets are at the end of the Research & Design phase. The testing of the short model magnets is almost finished and the next step is to manufacture and test the prototype magnets, which is followed by the series magnets. During my stage at CERN, I participated at the testing of MQXFS4c and MQXFS6b short model magnets.

The new focusing magnets will be made of Nb_3Sn superconducting wires. This material has very good properties, allowing to increase the aperture of the magnets and still providing high magnetic gradient for focusing. A drawback of this material is that it is very brittle and stress sensitive, therefore they have special magnetic and structural design as well as manufacturing process. The superconducting magnets also need to be tested in order to validate the design. The testing includes the cool-down of the magnets to cryogenic temperature (and also warming them up). During the cool-down the magnet shell shrinks more than the inner part of the magnet, which results in increased stress on the coils. The coils contain the superconducting wire, therefore it needs to be confirmed that during the testing processes, the coil is not damaged.

A detailed analysis of stress evolution during thermal transients (cooling and warming of the magnets) was done for MQXFS4 and MQXFS6 short model magnets tested at SM18 (CERN Magnets Test Facility). The magnets were equipped with strain gauges on the shell, rods and pole (coils) and with temperature sensors in different longitudinal positions on the shell. In total 5 different magnet assemblies were analysed during 22 thermal transients.

The analysis shows that the different models have similar behaviour during the thermal transients and the stress values are approaching the target values. For example the rod stress measurements are in the same value ranges for all of the magnets, and there are no main differences between cool-down and warm-up processes. In the case of shell stress measurements, the values had different behaviour during cool-down and warm-up: the lines were curved up for cool-downs and down during warm-ups. The coils had similar behaviour like the shell, however the absolute change in the stress values was lower. The stress measured on the coils never exceeded the critical value of 150 MPa.

The influence of many parameters was also taking into account. The analysis shows that the behaviour of stress was not related to cooling rate or temperature difference along the magnet in the ranges used during tests. The cooling rates were in range 7 - 21 K/h for cooling from room temperature to $\sim$ 80 K and 5 - 46 K/h when cooling from 80 - 4.5 K. The longitudinal differences in temperature were in range 20 - 50 K in the first step of cooling and 35 - 80 K in the second step. During warm-ups the temperature difference along the magnet was between 5 - 60 K. These cooling rates and temperature differences did not damaged the magnets.

The different behaviour in range of 80 - 4.5 K can be explained by the structural properties of the cryostats HFM and Cluster D and it's not related to the magnet itself. The different flow direction and movements of the cryogenic fluid are influenced by the cryostat parameters and shape. In HFM more space is between the magnet shell and the wall, for the magnets tested here, the shell stress measurements are flattened in 80 - 4.5 K range.

The similar behaviour in range 300 - 80 K for both cryostats could be caused by the fact that the strain gauge compensator and the sensor have delay in sensing the temperature change. This hypothesized sensing delay is confirmed by a passive warming of the MQXFS4c magnet in cluster D, when the stress measured on the shell was very similar to the cool-downs of other magnets tested in HFM.

This study can be extended to the study of all tested short model magnets for making more general conclusions. When the direct stress values are not available for the coils, a transfer function can be used, which gives the relation between shell stress and stress level in the coils. This function can be validated by comparing results of the transfer function with available coil strain measurements.

The aim of this study was the validation of the cool-down process at SM18 and the study of the evolution of the stress inside the MQXFS magnets during the thermal transients. The analysis confirms that the testing circumstances are suitable for the magnets in SM18, assuring that the stress level doesn't reach the critical value on the coils during thermal transients.

Bibliography

[1] G. Apollinari, O. Brüning, and L. Rossi, *High-Luminosity Large Hadron Collider (HL-LHC).* CERN, 2017. Technical Design Report v.0.1.

[2] Wikipedia, "Elementary particles of the Standard Model." `https://en.wikipedia.org/wiki/Particle_physics`. [Online; accessed 11-Feb-2020].

[3] O. S. Brüning *et al.*, *LHC Design Report.* CERN, 2004.

[4] CERN, "LHC - the guide." `https://home.cern/resources/brochure/cern/lhc-guide`, 2017. [Online; accessed 13-Sept-2019].

[5] R. Steerenberg, "Particle accelerators explained for everybody." `https://indico.cern.ch/event/821514/contributions/3434365/attachments/1924780/3185212/201910011_TE_Onboarding_Event.pdf`, 2019. [Online; accessed 11-Oct-2019; INDICO: 821514].

[6] "CERN's accelerator complex." `https://home.cern/science/accelerators/accelerator-complex`. [Online; accessed 18-Nov-2019].

[7] D. Schoerling, "Accelerator technology challenges (part 1: Magnet superconductivity)." `https://indico.cern.ch/category/345/`, 2019. presentations during Summer Student Lecture Programme Course - organized by CERN.

[8] CERN, "LHC magnet types." `http://lhc-machine-outreach.web.cern.ch/lhc-machine-outreach/components/magnets/types_of_magnets.htm`. [Online; accessed 05-Feb-2020].

[9] CERN, "HL-LHC WP3." `https://espace.cern.ch/HiLumi/WP3/SitePages/Home.aspx`. [Online; accessed 11-Nov-2019].

[10] CERN, "High Luminosity LHC project." `https://hilumilhc.web.cern.ch/`. [Online; accessed 05-Feb-2020].

[11] P. Ferracin, "Superconductivity and SC magnets for LHC upgrade." `https://indico.cern.ch/category/345/`, 2016. 2 presentations during Summer Student Lecture Programme Course - organized by CERN.

[12] S. I. Bermudez *et al.*, "Mechanical analysis of the Nb_3Sn 11 T dipole short models for the High Luminosity Large Hadron Collider," *Superconductor Science and Technology*, vol. 32, p. 085012, July 2019.

[13] E. Ravaioli *et al.*, "Towards an optimized coupling-loss induced quench protection system (CLIQ) for quadrupole magnets," *Physics Procedia*, vol. 67, pp. 215–220, 2015.

[14] D. Schoerling and A. V. Zlobin, *Nb_3Sn Accelerator Magnets.* Springer International Publishing, 2019.

[15] P. Ferracin *et al.*, "The HL-LHC low-β quadrupole magnet MQXF: From short models to long prototypes," *IEEE Transactions on Applied Superconductivity*, vol. 29, pp. 1–9, Aug. 2019.

[16] L. Rossi, "Manufacturing and testing of accelerator superconducting magnets," 2013. Comments: 30 pages, contribution to the CAS-CERN Accelerator School: Superconductivity for Accelerators, Erice, Italy, 24 April - 4 May 2013, edited by R. Bailey.

[17] S. I. Bermudez *et al.*, "Second-generation coil design of the Nb_3Sn low-β quadrupole for the High Luminosity LHC," *IEEE Transactions on Applied Superconductivity*, vol. 26, pp. 1–5, June 2016.

[18] S. Caspi *et al.*, "The use of pressurized bladders for stress control of superconducting magnets," *IEEE Transactions on Appiled Superconductivity*, vol. 11, pp. 2272–2275, Mar. 2001.

[19] E. Takala *et al.*, "Preload characterization of short models of MQXF the Nb_3Sn low-β quadrupole for the Hi-Lumi LHC," *IEEE Transactions on Applied Superconductivity*, vol. 30, pp. 1–6, June 2020.

[20] G. Chlachidze *et al.*, "Performance of the first short model 150-mm-aperture Nb_3Sn quadrupole MQXFS for the High-Luminosity LHC Upgrade," *IEEE Transactions on Applied Superconductivity*, vol. 27, pp. 1–5, June 2017.

[21] G. Vallone *et al.*, "Mechanical analysis of the short model magnets for the Nb_3Sn low-β quadrupole MQXF," *IEEE Transactions on Applied Superconductivity*, vol. 28, pp. 1–6, Apr. 2018.

[22] H. Bajas *et al.*, "Test result of the short models MQXFS3 and MQXFS5 for the HL-LHC upgrade," *IEEE Transactions on Applied Superconductivity*, vol. 28, pp. 1–6, Apr. 2018.

[23] F. Mangiarotti *et al.*, "Test results of the CERN HL-LHC low-β quadrupole short models MQXFS3c and MQXFS4," *IEEE Transactions on Applied Superconductivity*, vol. 29, pp. 1–5, Aug. 2019.

[24] G. Vallone *et al.*, "Summary of the mechanical performances of the 1.5 m long models of the $\mathrm{Nb_3Sn}$ low-β quadrupole MQXF," *IEEE Transactions on Applied Superconductivity*, vol. 29, pp. 1–5, Aug. 2019.

[25] G. Vallone *et al.*, "Mechanical performance of short models for MQXF, the nb3sn low-β quadrupole for the hi-lumi LHC," *IEEE Transactions on Applied Superconductivity*, vol. 27, pp. 1–6, June 2017.

[26] L. Bianchi, S. Emami, and M. Guinchard, "MQXFS6b mechanical measurements electrical vs. optical strain gauges." `https://edms.cern.ch/ui/#!master/navigator/document?D:100200387:100200387:subDocs`, 2020. presentation, EDMS no. 2019125.

[27] A. Chiuchiolo *et al.*, "Strain measurements with fiber bragg grating sensors in the short models of the HiLumi LHC low-beta quadrupole magnet MQXF," *IEEE Transactions on Applied Superconductivity*, vol. 28, pp. 1–5, June 2018.

[28] P. Grosclaude and M. Guinchard, "Strain measurements on MQXFS1 superconducting magnet - CERN & LARP comparative measurements." `https://edms.cern.ch/ui/file/2363920/1/Full_Report_LARP_CERN.pdf`, 2016. EN-MME Mechanical Measurement Lab Report, EDMS no. 2363920.

[29] Wikipedia, "Hooke's law." https://en.wikipedia.org/wiki/Hooke%27s_law. [Online; accessed 11-Mar-2020].

[30] M. Juchno *et al.*, "Mechanical qualification of the support structure for MQXF, the Nb_3Sn low-β quadrupole for the High Luminosity LHC," *IEEE Transactions on Applied Superconductivity*, vol. 26, pp. 1–6, June 2016.

[31] S. Emami, "MQXFS4a results." https://edms.cern.ch/ui/#!master/navigator/document?D:100064551:100064551:subDocs, 2019. EDMS no. 1906361.

[32] P. E. Bradley and R. Radebaugh, "Properties of selected materials at cryogenic temperatures." https://www.nist.gov/publications/properties-selected-materials-cryogenic-temperatures, 2013. [Online; accessed 28-May-2020].